AD-A180 099   1985 NATURAL LIGHTNING STUDY(U) MISSION RESEARCH CORP   1/1
ALBUQUERQUE NM   A H PAXTON ET AL   DEC 86 AMRC-R-760
AFWL-TN-86-23 F29601-85-C-0009

UNCLASSIFIED   F/G 4/1   NL
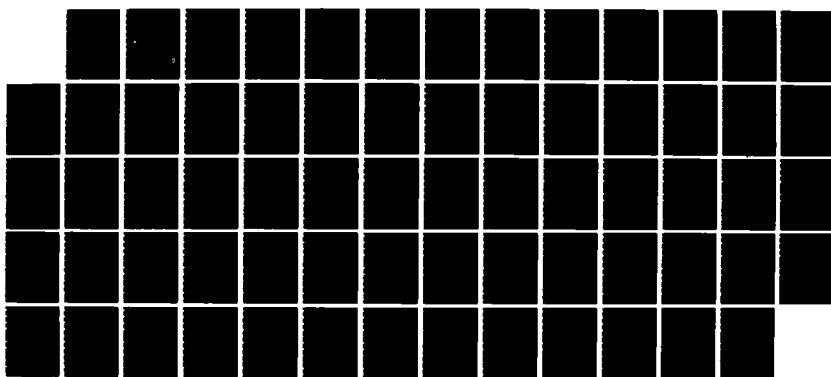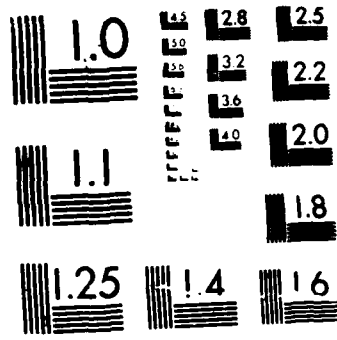
MICROCOPY RESOLUTION TEST CHART

NATIONAL BUREAU OF STANDARDS 1963 A

· DTIC FILE CUI· AFWL-TN-86-23

AD-A180 099

1985 NATURAL LIGHTNING STUDY

A. H. Paxton
L. Baker
R. L. Gardner

Mission Research Corporation
1720 Randolph Road SE
Albuquerque, NM 87106

December 1986

Final Report

DTIC
ELECTE
MAY 0 4 1987
S
E
D

AIR FORCE WEAPONS LABORATORY
Air Force Systems Command
Kirtland Air Force Base, NM   87117-6008

87   5   1   035

This final report was prepared by Mission Research Corporation, Albuquerque, New Mexico under Contract F29601-85-C-0009, Job Order 672A0911 with the Air Force Weapons Laboratory, Kirtland Air Force Base, New Mexico. Mr David H. Hilland (NTA) was the Laboratory Project Officer-in-Charge.

When Government drawings, specifications, or other data are used for any purpose other than in connection with a definitely Government-related procurement, the United States Government incurs no responsibility or any obligation whatsoever. The fact that the Government may have formulated or in any way supplied the said drawings, specifications, or other data, is not to be regarded by implication, or otherwise in any manner construed as licensing the holder or any other person or corporation, or as conveying any rights or permission to manufacture, use or sell any patented invention that may in any way be related thereto.

This report has been authored by a contractor of the United States Government. Accordingly, the United States Government retains a nonexclusive, royalty-free license to publish or reproduce the material contained herein, or allow others to do so, for the United States Government purposes.

This report has been reviewed by the Public Affairs Office and is releasable to the National Technical Information Services (NTIS). At NTIS, it will be available to the general public, including foreign nations.

If your address has changed, if you wish to be removed from our mailing list, or if your organization no longer employs the addressee, please notify AFWL/NTA, Kirtland AFB, NM 87117-6008 to help us maintain a current mailing list.

This technical report has been reviewed and is approved for publication.
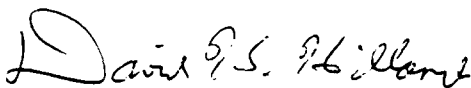
DAVID H. HILLAND
Porject Officer

FOR THE COMMANDER
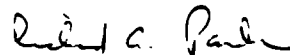
RICHARD A. PAULSEN   PHILIP J. MESSURI
Captain, USAF   Major, USAF
Chief, Technology Branch   Chief, Aircraft & Missiles Division
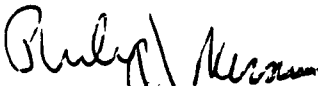
ADA180099

REPORT DOCUMENTATION PAGE

1a. REPORT SECURITY CLASSIFICATION	1b. RESTRICTIVE MARKINGS
UNCLASSIFIED	
2a. SECURITY CLASSIFICATION AUTHORITY	3. DISTRIBUTION/AVAILABILITY OF REPORT
	Approved for public release; distribution unlimited.
2b. DECLASSIFICATION/DOWNGRADING SCHEDULE	
4. PERFORMING ORGANIZATION REPORT NUMBER(S)	5. MONITORING ORGANIZATION REPORT NUMBER(S)
AMRC-R-760; MBES-2-MRC-041	AFWL-TN-86-23

6a. NAME OF PERFORMING ORGANIZATION	6b. OFFICE SYMBOL (If applicable)	7a. NAME OF MONITORING ORGANIZATION
Mission Research Corporation		Air Force Weapons Laboratory
6c. ADDRESS (City, State and ZIP Code)		7b. ADDRESS (City, State and ZIP Code)
1720 Randolph Road SE Albuquerque, New Mexico 87106		Kirtland Air Force Base, NM 87117-6008

8a. NAME OF FUNDING/SPONSORING ORGANIZATION	8b. OFFICE SYMBOL (If applicable)	9. PROCUREMENT INSTRUMENT IDENTIFICATION NUMBER
		F29601-85-C-0009

8c. ADDRESS (City, State and ZIP Code)	10. SOURCE OF FUNDING NOS.			
	PROGRAM ELEMENT NO.	PROJECT NO.	TASK NO.	WORK UNIT NO.
	64312F	672A	09	11

11. TITLE (Include Security Classification)
1985 NATURAL LIGHTNING STUDY

12. PERSONAL AUTHOR(S)
Paxton, A.H.; Baker, L.; and Gardner, R.L.

13a. TYPE OF REPORT	13b. TIME COVERED	14. DATE OF REPORT (Yr., Mo., Day)	15. PAGE COUNT
Final	FROM 2May85 TO 4Nov85	1986 November	68

16. SUPPLEMENTARY NOTATION

17. COSATI CODES			18. SUBJECT TERMS (Continue on reverse if necessary and identify by block number)
FIELD	GROUP	SUB GR	Lightning modeling Hydrodynamic modeling
04	01		Lightning

19. ABSTRACT (Continue on reverse if necessary and identify by block number)

The principal results of MRC's lightning research during 1985, including the collaborations with the Langmuir Laboratory of the New Mexico Institute of Mining and Technology and the Air Force Weapons Laboratory, Kirtland Air Force Base, are described.

Lightning strikes at the Kiva Facility of the Langmuir Laboratory have been observed and analyzed. The optical emissions and radiated electromagnetic field have been compared with computer simulations. The agreement is generally good. This facility is unique in the world, providing simultaneous measurements of stroke current, brightness, and radiated fields.

The major discovery has been that the initial return stroke velocity is approximately 0.9 c as opposed to average stroke velocities reported to be about 0.3 c.

20. DISTRIBUTION/AVAILABILITY OF ABSTRACT	21. ABSTRACT SECURITY CLASSIFICATION
UNCLASSIFIED/UNLIMITED ☒ SAME AS RPT ☐ DTIC USERS ☐	Unclassified

22a. NAME OF RESPONSIBLE INDIVIDUAL	22b. TELEPHONE NUMBER (Include Area Code)	22c. OFFICE SYMBOL
DAVID H. HILLAND	(505) 844-9758	NTA

DD FORM 1473, 83 APR   EDITION OF 1 JAN 73 IS OBSOLETE.

i

CONTENTS

ILLUSTRATIONS

ILLUSTRATIONS (Concluded)

TABLES

1. INTRODUCTION

Lightning is of interest to the Air Force for a number of reasons. It is a threat to aircraft, both in flight and on the ground. It is a threat to ground installations, particularly antennae and associated electronic equipment and power transmission lines. It is a potential spurious trigger of the Nuclear Detonation Detection System.

In addition to the reasons given above for the importance of natural lightning in its own right, an understanding of natural lightning is necessary as a basis for understanding nuclear lightning.

In order to characterize the threat posed by lightning, the important parameters are the (peak) current and the rate of current rise. Unfortunately, the observations of lightning to date do not provide a basis for confidently predicting or bounding these parameters. To rectify this situation, in an ongoing program involving the Air Force Weapons Laboratory (AFWL) and New Mexico Institute of Mining and Technology (New Mexico Tech) Langmuir Laboratory facility on South Baldy Peak, New Mexico, Mission Research Corporation (MRC) has begun a program to provide simultaneous observations of current, brightness, and radiated fields of a lightning stroke. The results of these initial efforts are described in this report. These results are unique, and provide valuable new insights into natural lightning. For the first time, there is evidence that the return stroke velocity is not a constant (typically reported in the literature as one-third that of light with a maximum observed value of about half the velocity of light), but is initially almost equal to the velocity of light and decreases with propagation up the channel. In addition, for the first time, there are correlated brightness and current observations. These are in good (but not perfect) agreement with computer calculations of the optical emissions based upon the observed current.

Sections 2 and 3 of this report describe the observation of visible light emission. Computational modeling is compared to observations in Section 3. Section 4 derives the relationship between observed intensity and intrinsic channel brightness used to analyze these observations.

1

Section 5 describes the analysis of the electromagnetic observations obtained
by B-dot and D-dot sensors located near the optical sensors. It was these
observations that revealed the high initial return stroke velocities.

Finally, Section 6 discusses theoretical analysis of experiments done
at the Langmuir Laboratory on the use of Primacord in the triggering of light-
ning. The aim of the experiment was to form a conducting channel rapidly by
detonating a length of Primacord suspended from a balloon. It was hoped that
this would provide a more realistic simulation of a natural lightning strike
to a tower than towing a conducting wire up with a rocket. This method did
not appear to provide a sufficiently conducting channel for an adequate time
to initiate a strike.

This work should serve as the foundation for a quantum leap in the
understanding of natural lightning. It should be possible, by applying and
extending the results of this study, to infer the current in a lightning
stroke by photographic observations; this should be of value in understanding
nuclear lightning. This work should lead to a better understanding of return
stroke initiation conditions and the development of the return stroke, leading
to better prediction of currents and rates of current rise. The threats posed
by lightning will then be better characterized.

2

2. DESCRIPTION OF LIGHTNING BRIGHTNESS EXPERIMENT

2.1 INTRODUCTION

The aim of the experiment was to record the light output of a small length of a lightning channel at the same time the current, electric field, and magnetic field were measured. This would be the first time such simultaneous observations were made. The time dependence of the light output was determined with a 10 ns time resolution, which was the resolution of the Biomation and Transiac digitizers that were available in Kiva 1. The photodiodes had a 5 ns resolution.

2.2 DESCRIPTION OF OBSERVATION SITE

The observations were performed at a facility at South Baldy Peak near the Langmuir Laboratory of New Mexico Tech. The facility includes a grounded aluminum mast penetrating the roof of an underground metal building, Kiva 2. The mast, which is 20 m long, is attached at its base to a lightning current measuring sensor array designed by EG&G. The array measures the electrical current, and its derivative dI/dt (Ref. 1). Two silicon photodiodes used for measuring optical radiation from lightning channels were located at a second underground building, Kiva 1. Electromagnetic sensors used to measure two horizontal components of dB/dt (B is the magnetic induction) and the vertical component of dD/dt (D is the electric displacement) are mounted to the roof of Kiva 1 (Ref. 2). The "ground plane" in the vicinity of Kiva 1 and Kiva 2 and between them is covered with a grounded wire mesh. A map of the facility is shown in Figure 1 taken from Ref. 3. The brightness experiment was designed by William Rison of New Mexico Tech and Carl E. Baum of the Air Force Weapons Laboratory in collaboration with the authors of this report.

The geometry for the brightness measurement is shown in Figure 2. The detector views an area centered 18 m above the mast of the current sensor array in order to decrease the likelihood that metal vapor would affect the

3
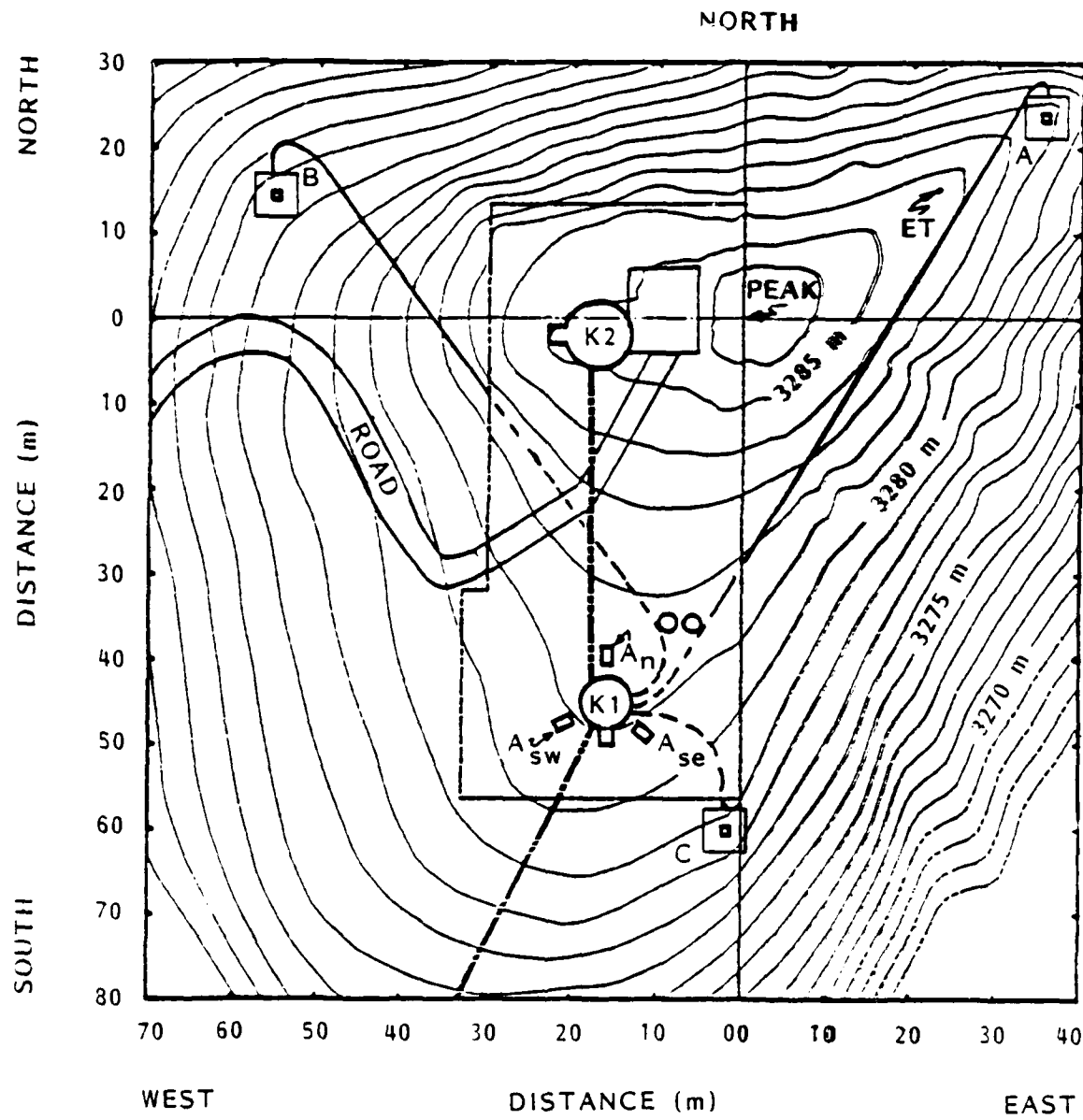
Figure 1. Map of the South Baldy facility. (from Ref. 3)

4
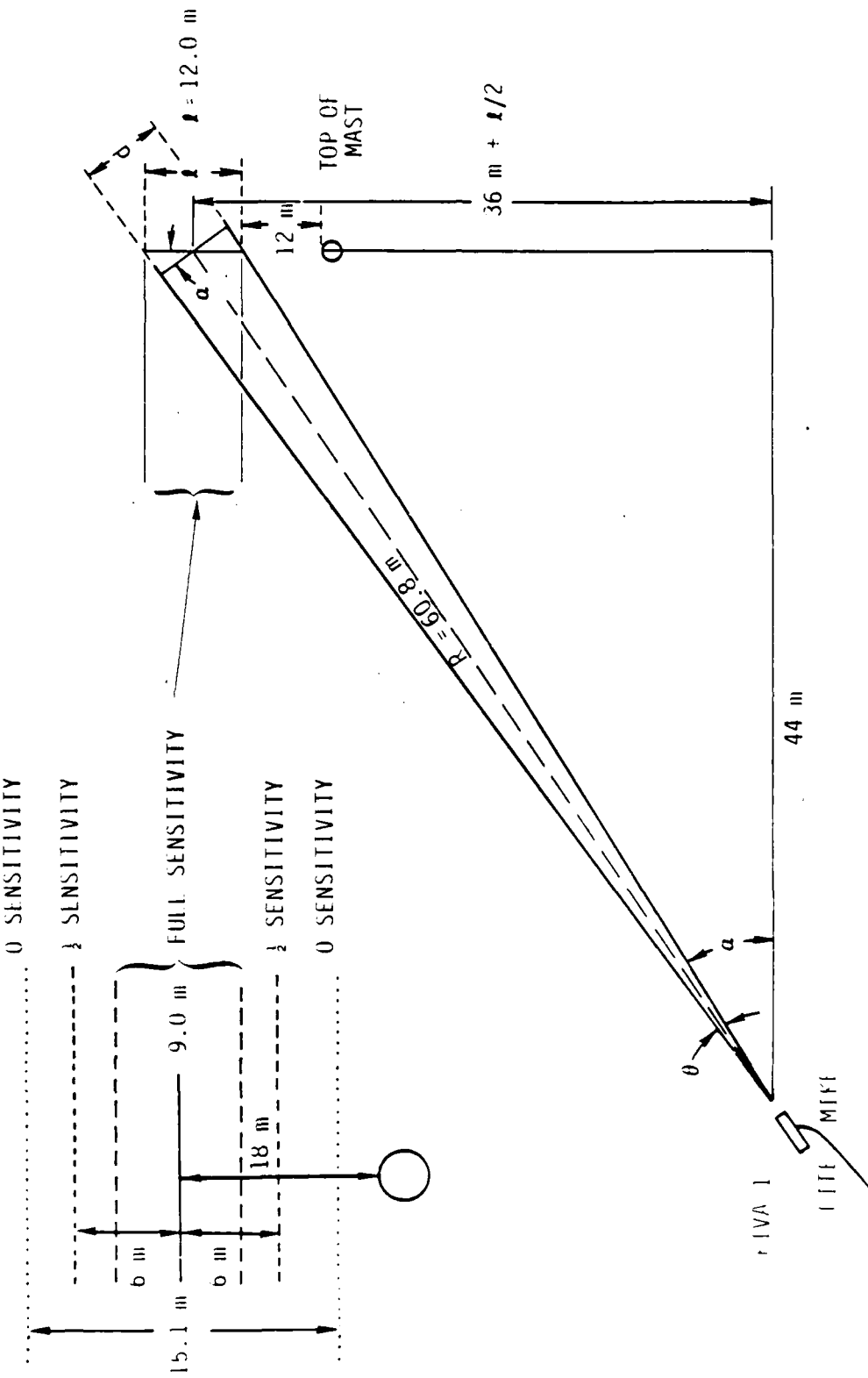
Figure 2.   Geometry for measuring the radiance per unit length of lightning channel.

light output from the channel. Assuming a vertical channel, the detectors
measured the brightness of a section of the channel that was 12.0 m long
between the half sensitivity points, 9.0 m long between full sensitivity
points, and 15.1 m long between zero sensitivity points. The section of
channel was centered at 18 m above the top of the mast of the current sen-
sor array mounted on Kiva 2. Collimators in front of the Lite Mike detec-
tors were designed so that the horizontal field of view was 17.4 m at a
distance of 60.8 m, twice as large as the vertical field of view; see Figure 3.
The Lite Mike detectors were configured in such a way that the center of
the field of view of each of them coincided with the center of the field
of view of a video camera that was mounted with them as a unit. The video
camera was used to aim the Lite Mike detectors. The metal box containing
the Lite Mike heads and the video camera was mounted in the crawl space
adjacent to Kiva 1, as is shown in Figure 4.

2.3 RELATION BETWEEN LITE MIKE VOLTAGE AND OPTICAL POWER
PER UNIT LENGTH RADIATED BY THE LIGHTNING CHANNEL

The switch on each Lite Mike detector head was set to the white X1
position, in order to match the impedance of the coaxial cables and the
digitizers. In this position, with the 50-Ω cables and a 50-Ω digitizer,
the calibration constant for either detector was 0.5 K_1, where K_1 is the
quoted calibration constant in volts per watt. The optical power values
were obtained as follows. The length of channel observed, assuming that it
was vertical, was ℓ = 12.0 m. The equation for the flux P in watts through
the surface of the photodiode at a given wavelength is

$$P (\lambda) = \frac{\ell W(\lambda)A}{4\pi R^2} \tag{1}$$

and the voltage is

$$V = \frac{K_1}{2} P \tag{2}$$

where A is the area of the photodiode, $W(\lambda)$ is the power radiated per unit
wavelength interval by a 1 m length of the channel, P is the convolution of
$P(\lambda)$ with the frequency response of the photodiode, and the factor of 1/2

SIDE VIEW

7 cm

1 cm

CONDUIT

INSIDE PAINTED FLAT BLACK

TO TRANSIAC
OR BIOMATION

TO LITE MIKE POWER
SUPPLY AND METER

CONDUIT

END VIEW

1 cm

RECTANGULAR
HOLE

2 cm

PHOTODETECTOR
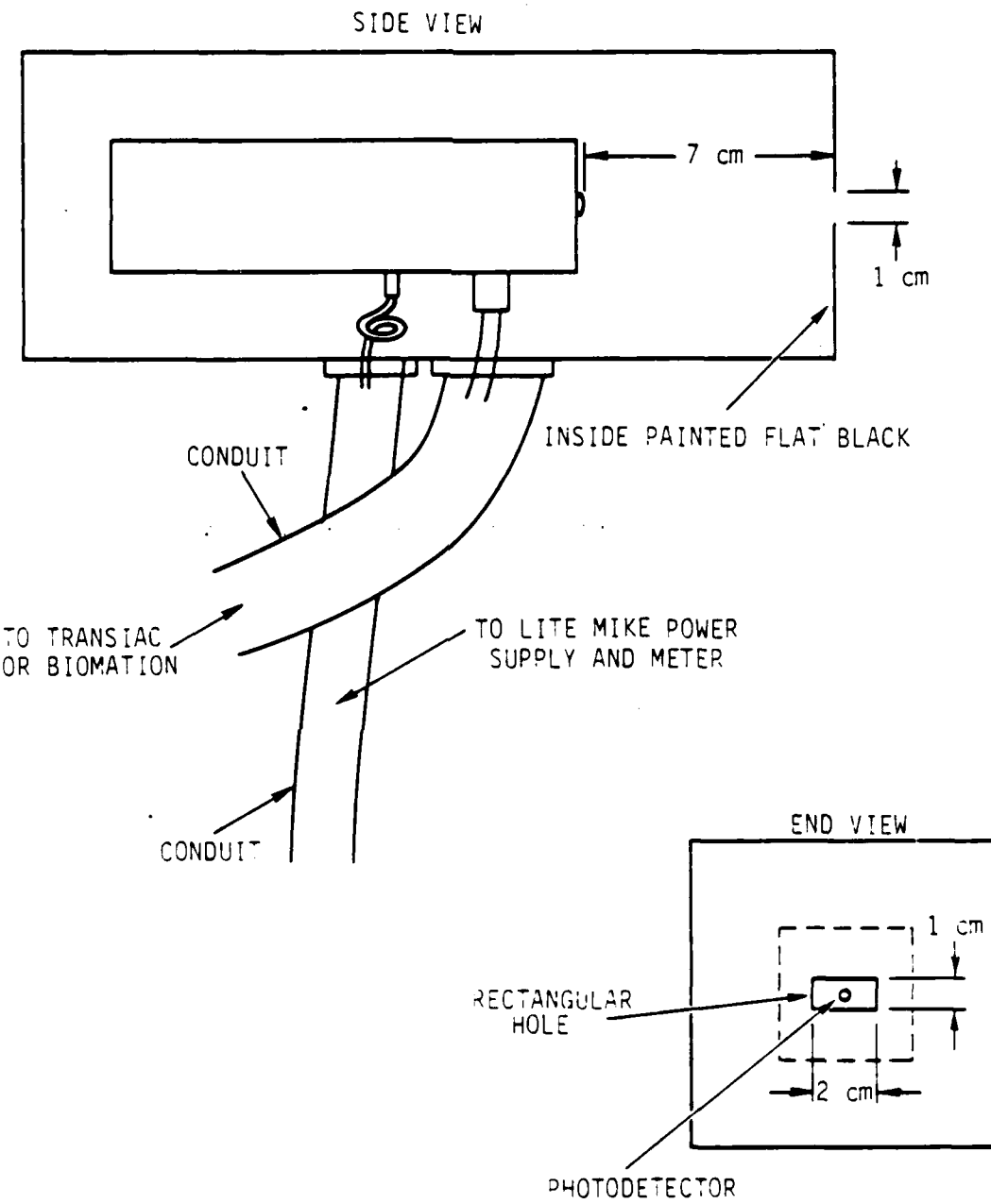
Figure 3. Collimator geometry for Lite Mike detector.
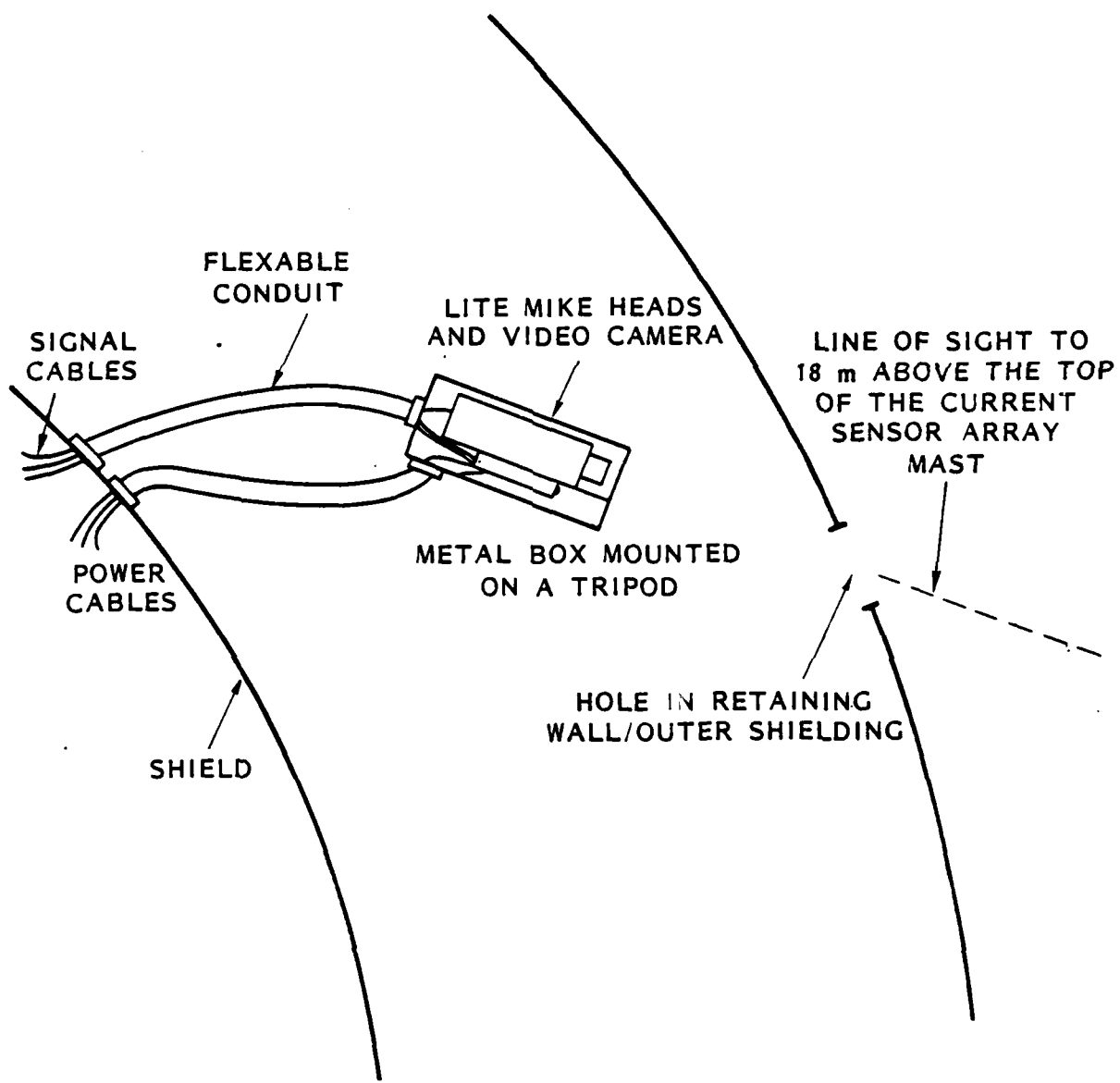
Figure 4. Lite Mike heads and video camera were located in the crawl
space adjacent to Kiva 1 to protect them from the weather.

arises because the lite mike output is impedance matched rather than connected to an infinite impedance. The value of K_1 corresponding to the Lite Mike with product serial no. 0272 is 30.20 V/W, and the photodiode has area, $A = 0.0507$ cm^2. The product $K_1 A$ is 1.24 V·cm^2/W for the other Lite Mike, serial no. 0420, $K_1 A = 1.53$ V·cm^2/W.

3. CHANNEL BRIGHTNESS CALCULATIONS

3.1 INTRODUCTION

The CHARTB one-dimensional magnetohydrodynamic (MHD) code was used to simulate the optical radiation emitted by the channel. CHARTB was developed at Sandia National Laboratories. It is a state-of-the-art program, containing approximately 12000 lines of FORTRAN code. It includes a tabular equation-of-state for air. A fully consistent calculation of the current profile in the channel (incorporating magnetic diffusion and advection) is performed and the Lorentz force is included. In air and other gases, CHARTB has been used to model the action an explosive opening switch, to simulate exploding wires and to solve various other problems with good results. CHARTB has been used to simulate the evolution of plasma channels for particle beam transport.

In each case, the lightning calculations were begun with an initial channel temperature of 1 eV and a channel with a 1 mm radius. The current was specified by the equation

$$I = I_0[\exp(-t/t_f) - \exp(-t/t_r)] \tag{3}$$

where t is the time and the constants t_r, t_f, and I_0 were selected to match Equation 3 as closely as possible to the measured current.

3.2 RADIATIVE TRANSPORT

CHARTB contains a multigroup radiative transport algorithm using the diffusion approximation, which was used to calculate the power of the optical radiation in the band of sensitivity of the EG&G Lite Mike detector that was used to measure the optical power radiated per unit length by the lightning channels. The radiative transport algorithm used is described in detail in Ref. 4. The spectrum of optical radiation was divided into frequency intervals, or groups. The group boundaries were selected to minimize the opacity variation within each group. A single value of the

10

opacity was assigned to each group using the Rosseland mean. This type of average is more accurate for the optically thick case, in which the radiation is absorbed and reradiated a number of times in traversing the calculational grid, than for the optically thin case. In the limit in which groups are narrow enough to resolve the opacity versus frequency function, the algorithm used is valid in both the optically thick and optically thin limits. Optical radiation is the dominant mechanism of energy transfer from the hot conducting gas to the cooler gas in the outer part of the channel.

The diffusion approximation is also known as the P_1 method, which refers to the first-order expansion of the intensity in spherical harmonics. With the Marshak boundary condition, which we used, this approximation gives radiant energy densities that are accurate in the optically thick limit, but the energy densities are overestimated in the optically thin limit. However, the power radiated by the hot part of the channel is almost independent of the radiant energy density for optically thin bands, and the energy in thin bands that is reabsorbed in the cooler gas is a negligible fraction of the energy radiated in the hot region. Therefore, large errors would result if the calculated output flux at the edge of the grid had been used to obtain the radiated power in the band of interest, but by summing the net radiated power over all grid zones, accurate results were obtained.

The radiant field is completely specified by the intensity function, $I(t,\vec{r},\vec{\alpha},\nu)$, where t is the time, $\vec{r}$ is the location, $\vec{\alpha}$ is a unit vector in the direction of travel, and ν is the frequency. At a point interior to the lightning channel, the light that is radiated by the gas in a differential volume will travel away in all directions. Light also arrives at the point from all directions, and any ray that passes through the differential volume is partially absorbed. The intensity $I(t,\vec{r},\vec{\alpha},\nu)d\Omega d\nu$ ($W/m^2 srH_z$) is the flux with frequency between ν and $\nu + d\nu$ within solid angle $d\Omega$ of a light ray with direction $\vec{\alpha}$ (see Figure 5). The light ray passes through point $\vec{r}$.
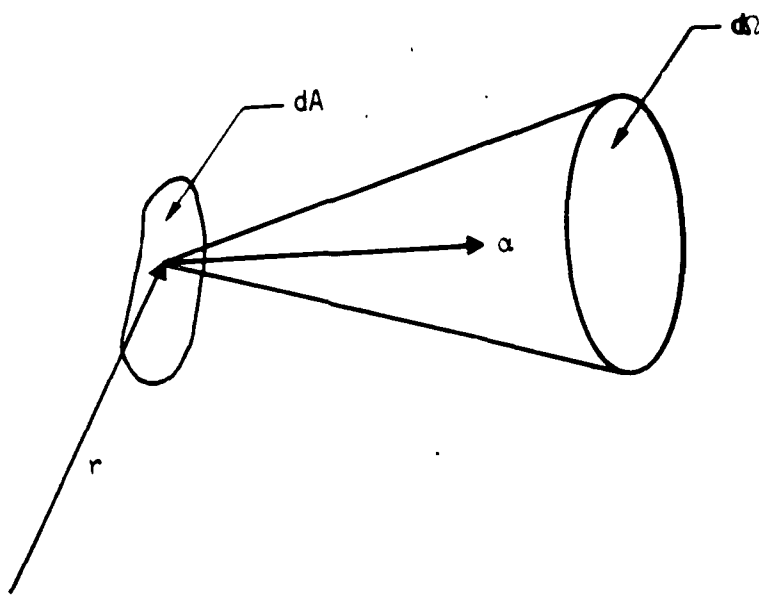
Figure 5. Illustration of the vectors and differential elements that specify the intensity function.

The equation of radiative transfer is

$$\dot{I} \equiv \left(\frac{\partial}{\partial t} + c\vec{\alpha} \cdot \triangledown \right) I = \text{Sources} - \text{Sinks} .$$ (4)

The convective derivative of the intensity function is the intensity created minus the intensity absorbed. The sinks are

$$\text{Sinks} = c(k_{abs} + k_{scat}) I .$$ (5)

The intensity loss due to scattering from one frequency to another is included in k_{scat}. The frequency- and temperature-dependent absorption coefficient per unit distance is k_{abs}. The source terms are

$$\text{Source} = ck_{abs} B(T,\nu) + S_{scat}$$ (6)

where

$$B(T\nu) = \frac{2}{c^2} \frac{h\nu^3}{e^{h\nu/KT} - 1} .$$

12

S_{scat} is the intensity gain due to scattering from one frequency to another and $ck_{abs} B(T,\nu)$ is the rate of increase of the intensity due to the emitted radiation. $B(T,\nu)$ is the Planck function for the blackbody intensity spectrum. The scattering terms are small compared to the absorptivities and may therefore be neglected.

Ignoring the scattering terms, Equation 4 becomes

$$\left(\frac{\partial}{\partial t} + c\vec{\alpha} \cdot \nabla\right) I = ck_{abs} \left(B(T,\nu) - I\right). \tag{7}$$

In the optically thick steady-state case in which absorption exactly cancels emission, $I = B(T,\nu)$. In the optically thin limit, $I \ll B(T,\nu)$ and the emission rate is simply

$$\dot{I} = ck_{abs} \ B(T,\nu). \tag{8}$$

This equation justifies our lack of concern for the accuracy of I for optically thin bands, for which $I \ll B(T,\nu)$. Equation 7 was used to obtain the radiated power in each volume element rather than obtaining the radiated output from the outward component of I at the edge of the grid.

The diffusion approximation of Equation 7 is obtained in terms of the energy density of the radiation field, $U = 1/c \int I d\Omega$. By assuming that I is nearly isotropic, the diffusion approximation is obtained (Ref. 4).

$$\left(\frac{1}{c}\frac{\partial}{\partial t} - \nabla \cdot \frac{1}{3k_{abs}} \nabla\right) U = k_{abs}\left(\frac{4\pi}{c} \ B(T,\nu) - U\right). \tag{9}$$

At the center of the coordinate system, the boundary condition $\partial U/\partial r = 0$ was applied. The boundary condition applied at the edge of the grid is a Marshack condition of the form

$$\frac{2}{3k_{abs}} \ \frac{\partial U}{\partial r} + U = 0. \tag{10}$$

A standard tridiagonal finite-difference algorithm was used to solve Equation 9 numerically.

Spectral lines were not treated individually, but were included in the continuum absorptivities. Their contributions to the opacities were therefore somewhat overemphasized (Refs. 5, 6). The opacity tables of Ref. 6 were used in the calculations.

3.3   CALCULATED PROPERTIES

The first lightning strike that was triggered at the South Baldy facility, designated #85220, had a peak current of about 17 kA with a rise time $t_r = 2.4 \times 10^{-7}$ s. I_0 and t_r were given these values for the numerical simulation, and the decay time was given a value $t_f = 2.5 \times 10^{-5}$ s. The time duration used for the simulation was 5 µs. The measured current is shown in Fig. 6 and the current pulse shape assumed for the calculation is shown in Fig. 7.

Radial current profiles, temperature profiles, density profiles, and pressure profiles were generated. The temperature profiles are shown at times of 1.0 µs , 2.0 µs and 5.0 µs in Fig. 8. It is seen that the temperature profile has a dip in the center at very short times. This shape is probably caused by the assumed initial channel temperature distribution. by a time of 2 µs, the dip is gone and the temperature distribution is highest at the center.

The current density plots, Fig. 9, display some interesting features. The conductivity of the air experiences a sharp cutoff as the temperature drops below about 2 eV. Therefore the current is confined to the region with a temperature above 2 eV. The current "spike" that occurs near the outside of the hot channel is caused by the small skin depth of the hot channel gas. As the time derivative of the current decreases, the skin depth of the current increases and the outer layer of increased current thickens, as is seen in the plots.

The density and pressure plots, Figs. 10 and 11, show a shock wave propagating outward at the edge of the channel. At longer times than were used in the calculations, the shock wave separates from the channel of hot gas and travels outward through the cool air.

14
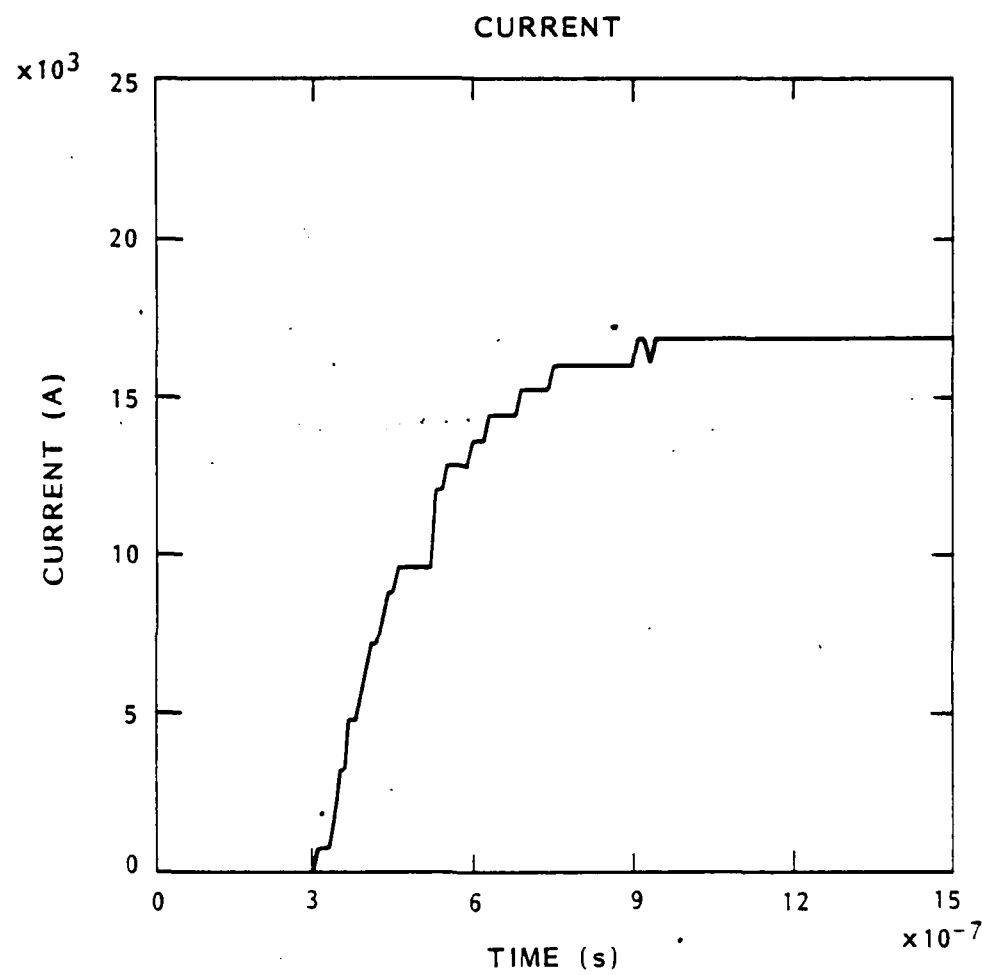
Figure 6. Measured current of lightning stroke no. 85220.
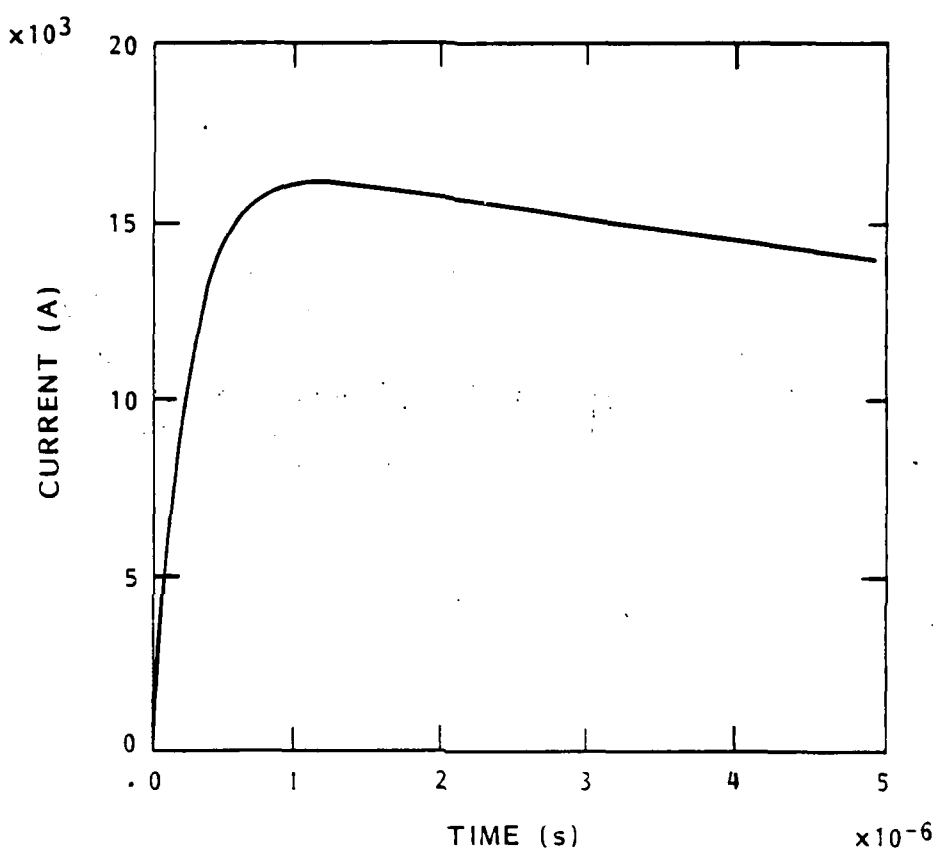
Figure 7. Current waveform used to simulate stroke no. 35220.

(a) TIME, 1 μs (b) TIME, 2 μs
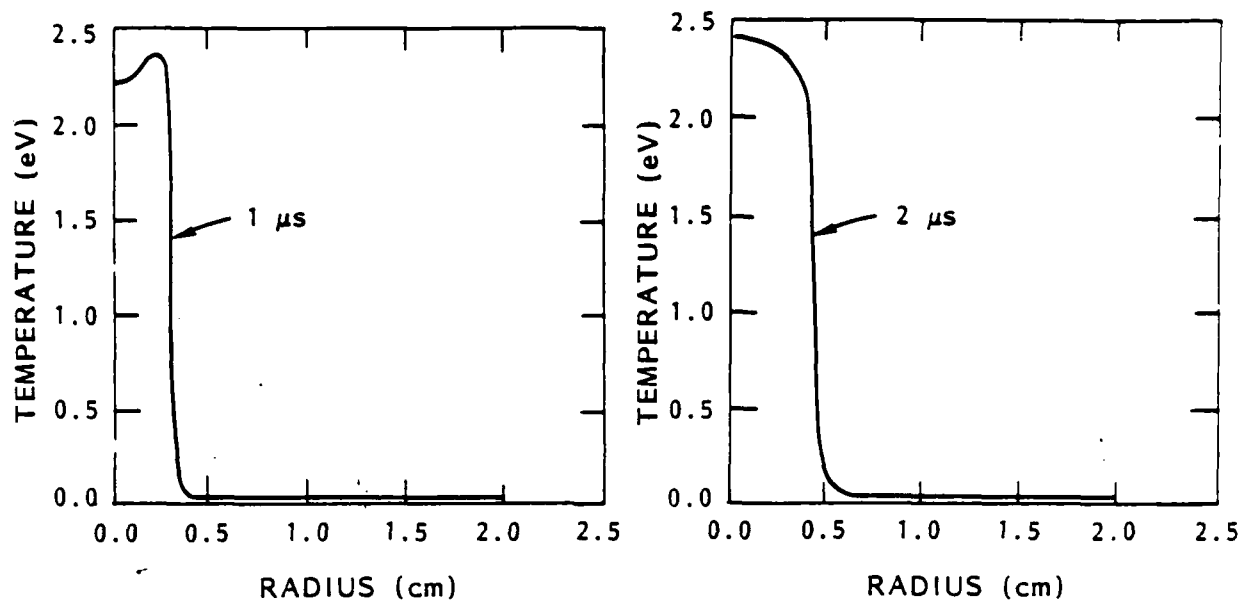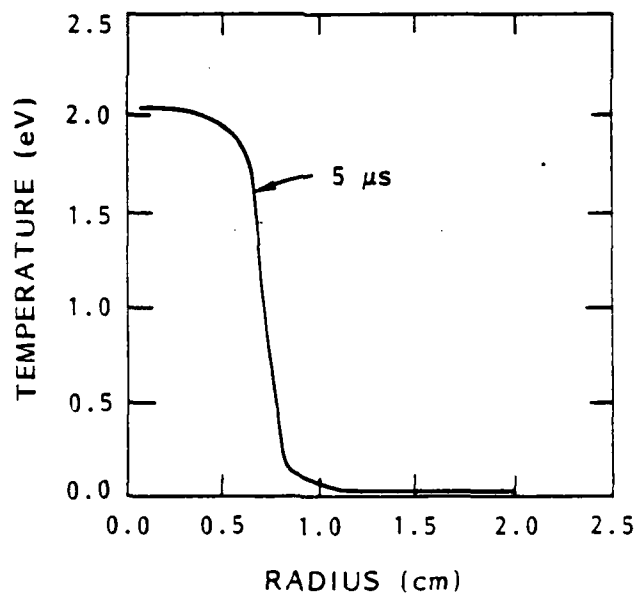
(c) TIME, 5 μs

Figure 8.   Calculated temperature profiles at three times.
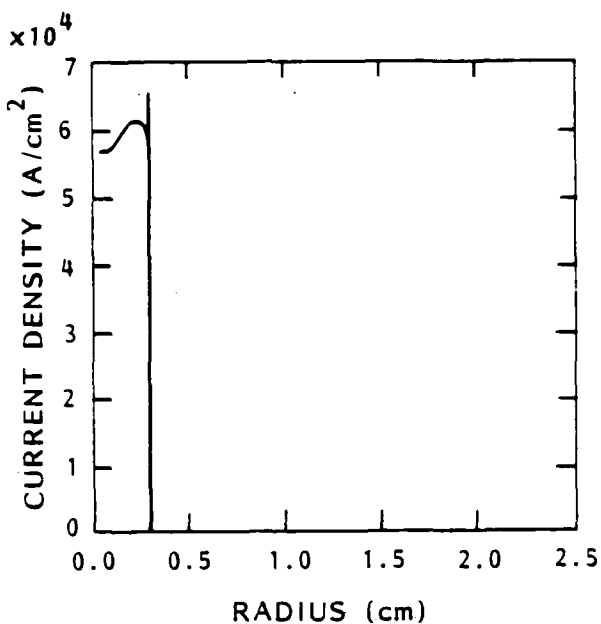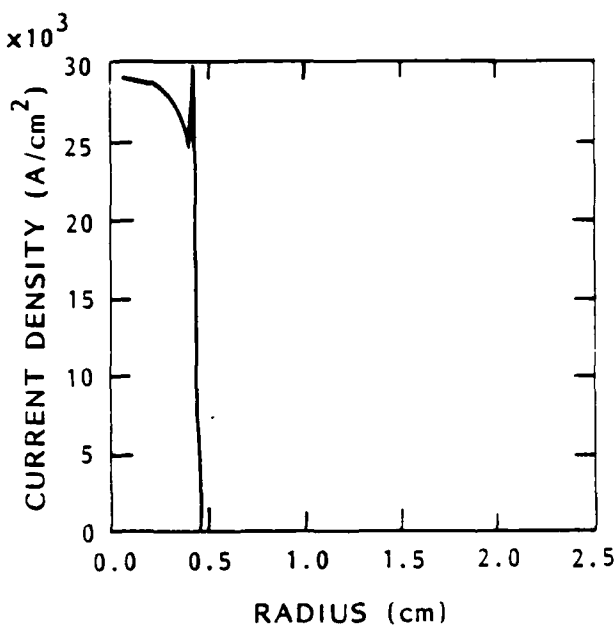
(a) TIME, 1 μs
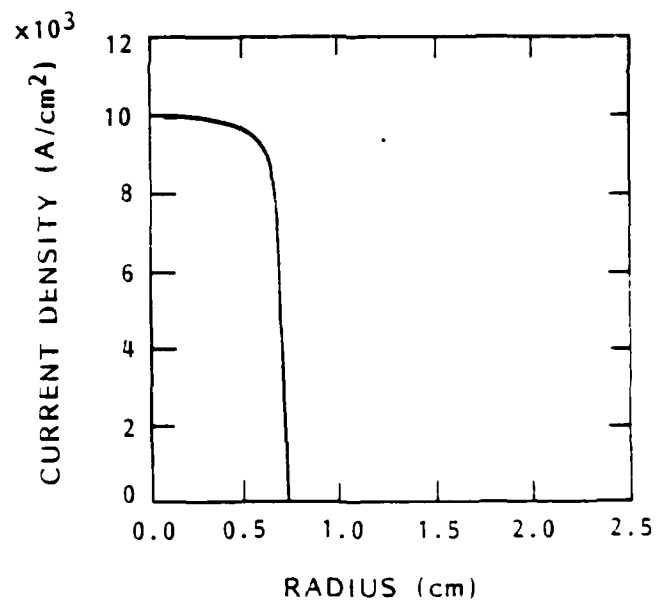
(b) TIME, 2 μs

(c) TIME, 5 μs

Figure 9. Calculated current density profiles at three times.

18

(a) TIME, 1 μs
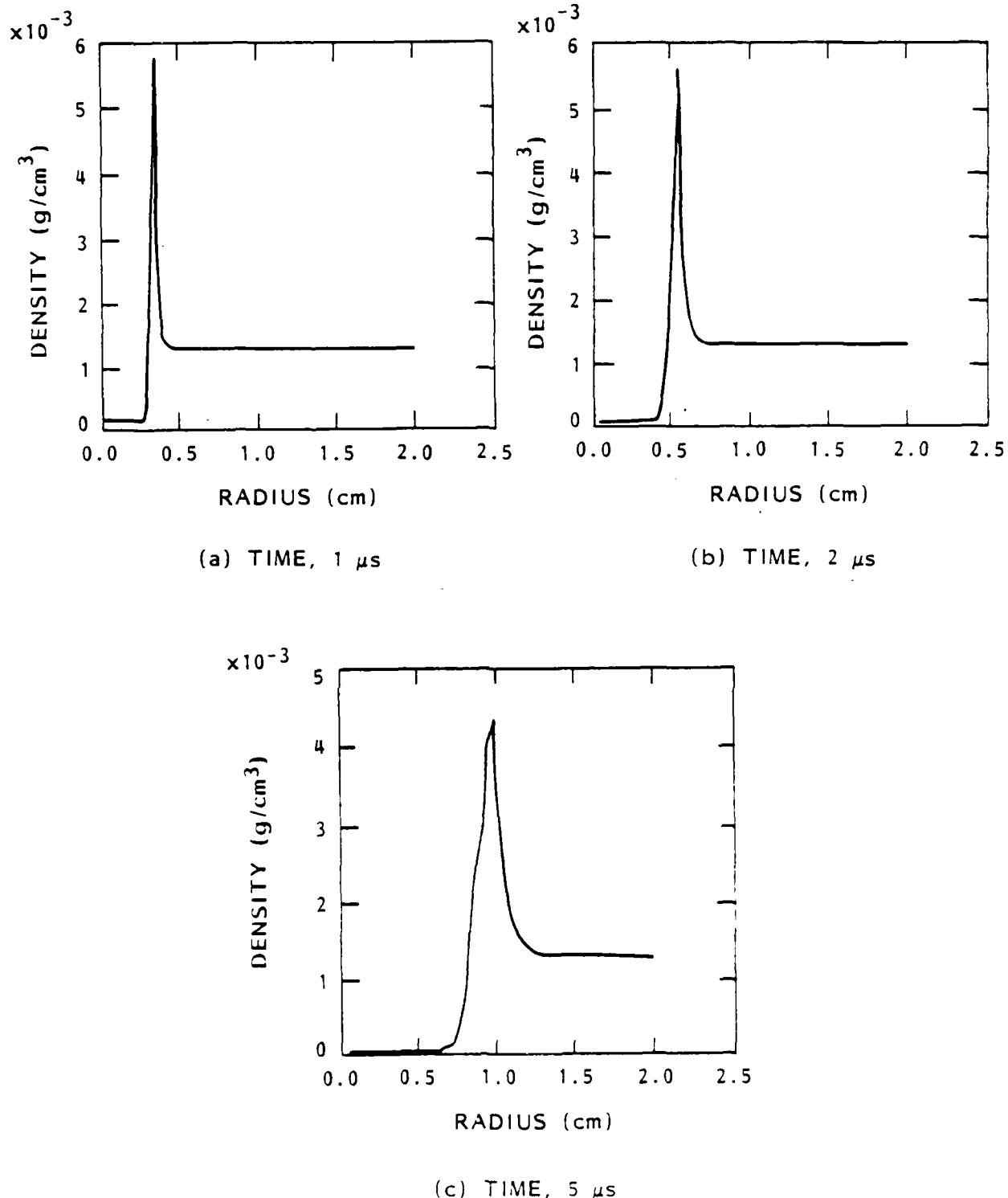
(b) TIME, 2 μs

(c) TIME, 5 μs

Figure 10. Calculated density profiles at three times.
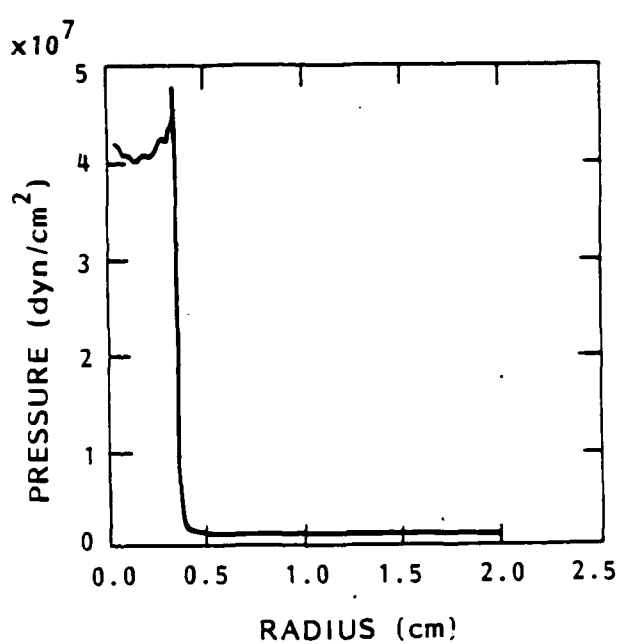
(a) TIME, 1 μs
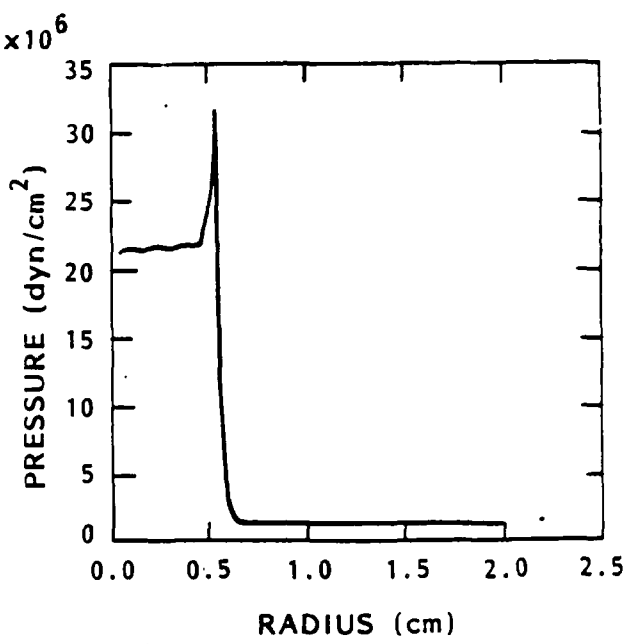
(b) TIME, 2 μs
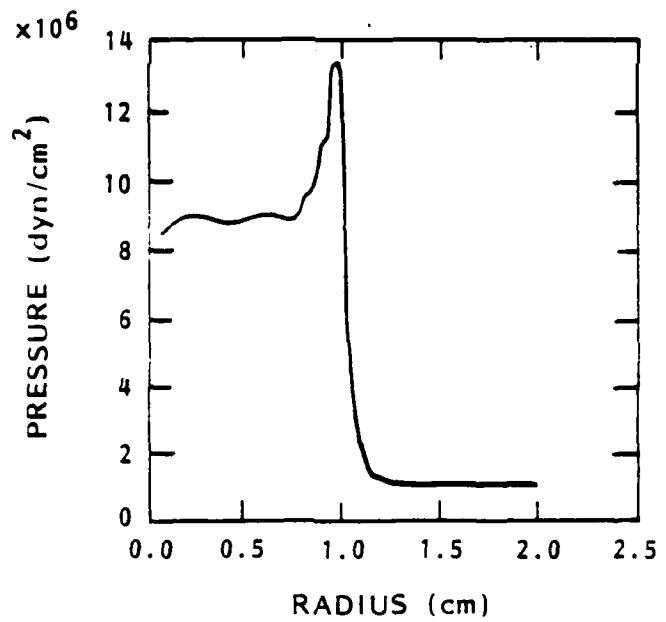
(c) TIME, 5 μs

Figure 11. Calculated pressure profiles at three times.

20

The calculated optical emission of the channel was obtained by convolving the detector response curve of the Lite Mike detector with the calculated frequency spectrum of the radiated light. It would be prohibitively expensive to use enough frequency groups to calculate the frequency spectrum of the radiated light with adequate resolution for convolution with the detector sensitivity curve. Therefore, the radiated light was assumed to have a Planck distribution at the temperature of the radiating cell, within the group that contained the detector response curve. This group covered the 1.0 to 3.0 eV frequency interval. The calculated emission and the measured emission are shown in Figure 12. The calculated emission rises to a peak of 11 MW/m, then falls to about 4.5 MW/m while the current remains almost constant. The measured optical emission, however, rises to about 3.7 MW/m and then remains constant for the 1.5 μs shown on the plot. This discrepancy probably results from the initial conditions selected for the calculation. The CHARTB computer code does not contain an electrical breakdown model, but begins the calculation with an initial small hot channel. The size and temperature of this initial channel affects the radiated output for times of a few microseconds. An interesting area for future research would be the application of gas breakdown theory to the determination of appropriate initial conditions for MHD programs, such as CHARTB.

The light output from a second lightning stroke was also calculated. The measured current is shown in Figure 13 and the current waveform used in the calculation is shown in Figure 14. The calculated optical emission convolved with the detector sensitivity and the measured optical emission are shown in Figure 15. The calculated output at a time of 1 μs is about 6 MW/m, while the measured value is 5 MW/m. This is very good agreement. The spike at the origin of Figure 16 is probably dependent on the initial channel temperature distribution used in the calculations.
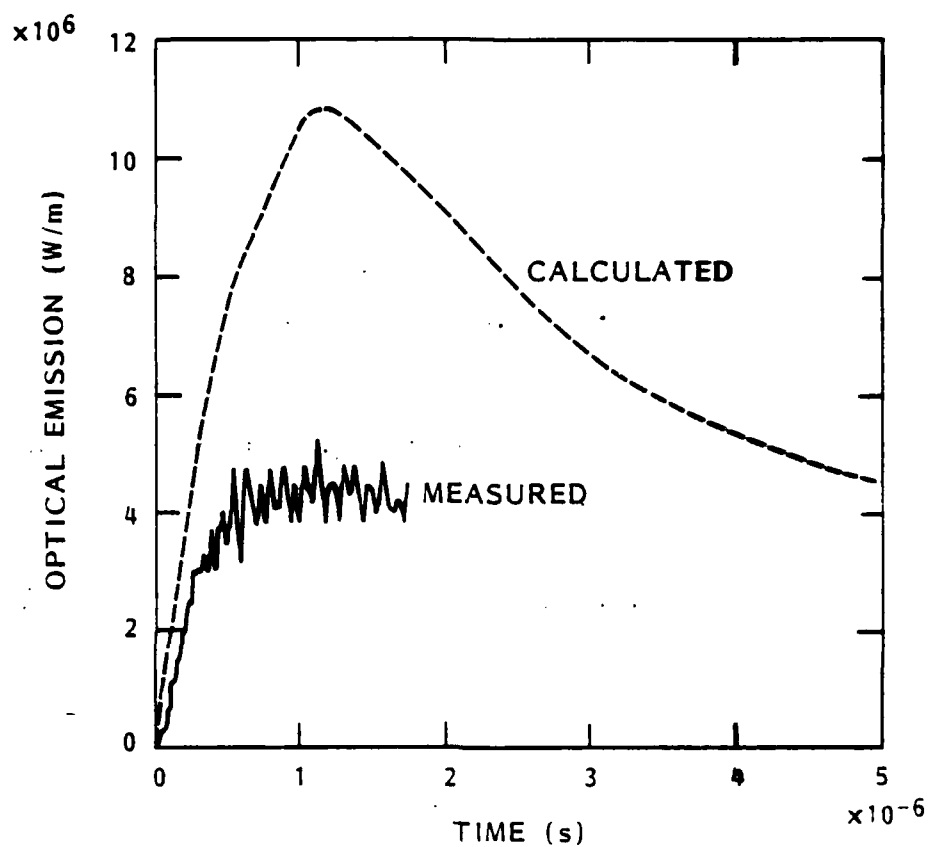
Figure 12. Calculated and measured optical emission from lightning stroke no. 85220.
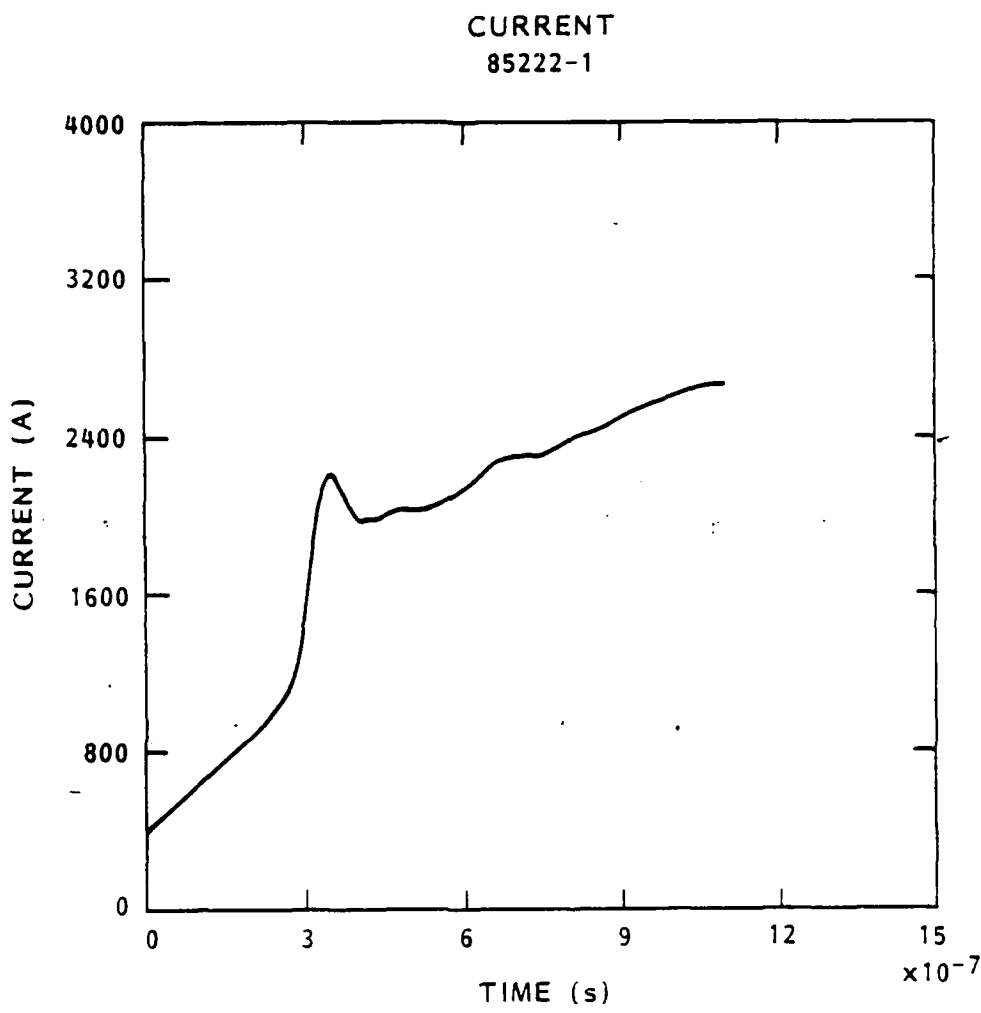
CURRENT
85222-1

Figure 13. Measured current of lightning stroke no. 85222-1.

23
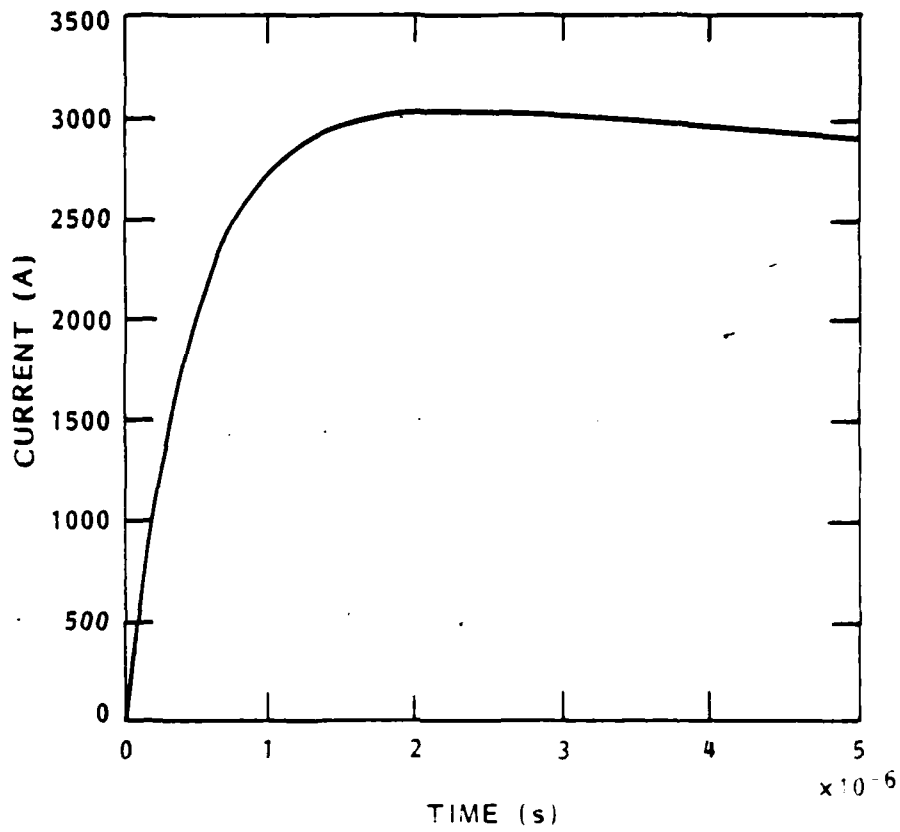
Figure 14. Current waveform used to simulate lightning stroke no. 35000-1.
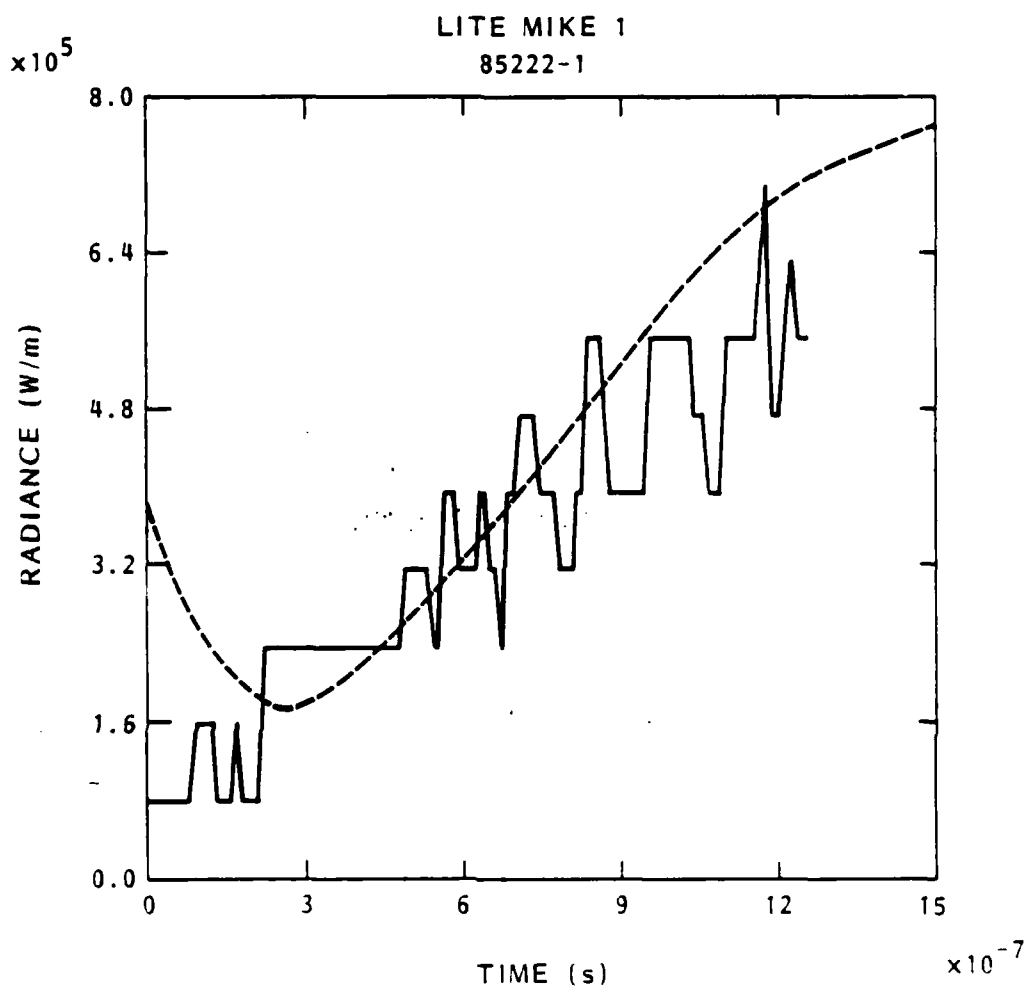
Figure 15. Calculated and measured optical emission from lightning stroke no. 85222-1. Solid curve shows measured values and dashed curve shows calculated results.

4. RELATION OF CHANNEL LUMINOSITY TO IRRADIANCE AT LITE-MIKE

4.1 INTRODUCTION

Optical observations are used to determine the illuminance
(in lm/m^2), or equivalently the irradiance (in W/m^2). The subject of this
section is how to obtain from this information the channel luminosity per
unit length (in W/m). This is done as two separate problems: (1) relating
the channel's optical properties to the luminance and then the brightness
at the film (or detector), and (2) relating the luminance to the luminosity
or radiation per unit length. We will show that the relationships between
channel luminosity and observed brightness for optically thick and thin ·
channels differ only slightly. We will develop the theory by treating pro-
gressively more complex radiators: a plane, Lambert's law radiator, a
plane, non-Lambertian surface, a cylindrical Lambert's law radiator, and
lastly an optically thin cylinder.

4.2 THEORY

4.2.1 Simple Plane Radiator

Because we have found inconsistencies between definitions of luminance
between references (Refs. 7-9) and because some derivations do not list
underlying assumptions (Lambert's law), we feel it is useful to define
terms and to treat first the simple case of the image brightness of a plane
surface of infinitesimal area, perpendicular to the line-of-sight. We con-
sider first a surface satisfying Lambert's law, such as a black body or
optically thick radiator. Then we will consider the effect of relaxing
this assumption. Finally, we will turn to the geometry of interest, that
of an infinite cylinder.

We will use SI units for radiometric quantities. Note that radiant
sterance was formerly called radiance and radiant incidence was called
irradiance. To convert to photometric quantities, one would use lumens

26

instead of watts in all quantities; radiant flux would become luminous flux, radiant incidence (irradiance) becomes illuminance, radiant sterance (radiance) becomes luminance, etc. Knowing the spectral distribution of the radiation, one can convert from one system to the other using the standard luminous efficiency curve (e.g., Ref. 9 graph, p. 39, table p. 40). Table 1 describes our notation. As we do not consider any electromagnetic variables, no confusion should arise about the variable used. The variables are listed in order of appearance in the text.

Larmore (Ref. 8) finds the radiant incidence at the lens (retaining his notation but changing from his photometric units to radiometric units) $I = EA/(\pi R^2)$, where E is the radiant exitance (formerly emittance or radiant flux density) at the source (in W/m^2), A is the surface area (m^2), and R (m) is the distance between the emitter and the lens (Fig. 16). We may relate the radiant incidence E at the source and the radiant sterance L in $(W/m^2/sr)$, in the notation of (Ref. 9), by integrating over the angle θ between the surface normal and the direction of emission (line of sight). If Lambert's law holds, the radiant intensity (W/sr) is proportional to $\cos(\theta)$ and the radiant sterance L is independent of θ. Then

$$E = 2 \pi \int_0^{\pi/2} L(\theta=0) \cos(\theta) \sin(\theta) \, d\theta.$$
$$= \pi L \tag{11}$$

Page 167 of Ref. 9 gives as the radiant flux F at the lens $F = \pi LA [\sin(q)]^2$, where q is the half-angle subtended by the camera entrance pupil at the emitter. We should have $I = F/[\pi(D/2)^2]$, where D is the lens diameter. For $D \ll R$, we have $\sin(q) \approx D/2R$. We find $I = LA/R^2$ which indeed checks with the results of Ref. 2.

TABLE 1. RADIOMETRIC QUANTITIES

Variable	Units	Term
I	W/m^2	Radiant incidence (irradiance) (at entrance pupil)
L	$W/m^2/sr$	Radiant intensity
E	W/m^2	Radiant exitance
F	W	Radiant flux
i	W/m^2	Radiant incidence (image)
W	W/m	
ε	W/m^3	Volume emissivity
B	W/m	

t,e,h are dimensionless factors
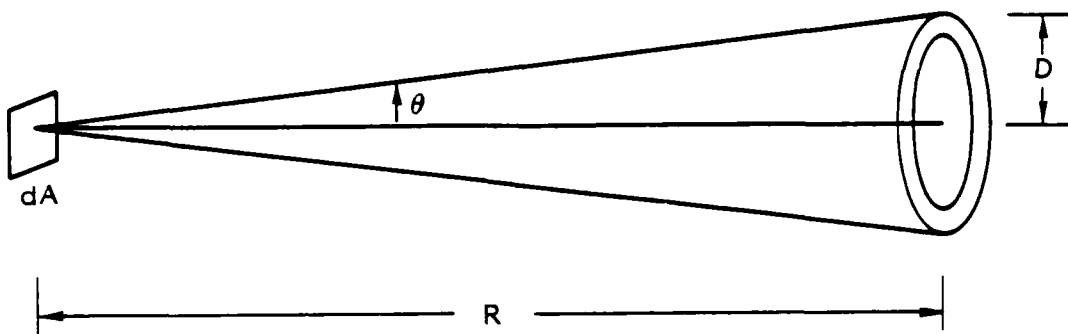
Figure 16. Geometry for illumination of detector by planar radiator.

We now relate the flux or flux density (exitance) at the lens to the image brightness at the film. This is $i = F/a$ where a is the area of the image. We have $i = I\pi D^2/4a = EAD^2/4aR^2$. As the magnification m is related to the areas A and a and the optical system's focal length f by $m^2 = a/A = (f/R)^2$ we have $i = ED^2/4f^2$, as given by Larmore (Ref. 8). Note that the results are independent of the distance between the source and the film. Note also that we have neglected transmission losses, both within the optical system as well as between the source and the camera. These losses will be accounted for by a simple multiplier.

For a plane radiator, we are concerned with a radiative loss rate E in (W/m^2) but not a loss per unit length. In this case we have simply related i and E and no more work need be done. We might write $E = 4i_+t\ (f/D)^2$ where t is the net transmission factor for the atmosphere and f/D is the f-stop of the optical system. This would solve our task of relating E to i.

29

4.3 NON-LAMBERTIAN RADIATOR: OPTICALLY-THIN PLANE SLAB

If the plane emitter is not a blackbody source, but, e.g., an optically thin layer of emitting gas, we would find in place of Lambert's law (L independent of θ), L ~ sec θ due to path length. The radiant intensity would be independent of θ, as the factors of sec θ and cos θ would cancel. Then we have $L(\theta=0) = E/2\pi$, and ultimately $E = 8i/t(f/D)^2$. This is a factor of two different from our previous results. Finite optical-depth sources will be intermediate between the two cases presented here, a factor of the form $1 + \exp(-d)$ where d is the optical thickness of the slab, may be used as an approximate interpolation factor. Note that, because of the small angle approximation, the departure from Lambert's law does not materially affect the relationship between i and I or between I and L, only the relationship between E and L.

4.4 INFINITE CYLINDER, LAMBERT'S LAW RADIATOR

We now proceed to develop similar results for an infinite cylinder. Applying the formalism of Ref. 9, we have:

$$F = 2r \int_0^{\ell} dz \int_0^{\pi/2} d\theta \int_0^{2\pi} d\phi \int_0^{q} [\cos \psi \, L(\psi)] \sin (a) \, da$$

where the angles are defined in Figure 17. The small angle approximations simplify things considerably, as the cosine of any small angle may be taken as 1, to first order. Then $\psi = r/R \sin \theta - \sin a = (1 + r/R)\theta - a = \theta$ to the required accuracy. Consider a section of the channel of length 1 for concreteness. We then find $F = \pi L \, 2r\ell \sin^2(q)$, i.e., the the same as for a plane surface emitter with the same projected area (area perpendicular to the line of sight), as we might have expected. Setting the projected channel area $A = 2r\ell$, we have again $I = LA/R^2$ and $i = L \, \pi/4 \, (D/f)^2$, but now instead of $L = E/\pi$ we have to relate L to a loss rate per unit channel length. For an optically thick channel we have W (W/m) $= 2\pi \, rS$ where the emission rate per unit of surface area is $S - \sigma T^4$ and σ is the Stefan
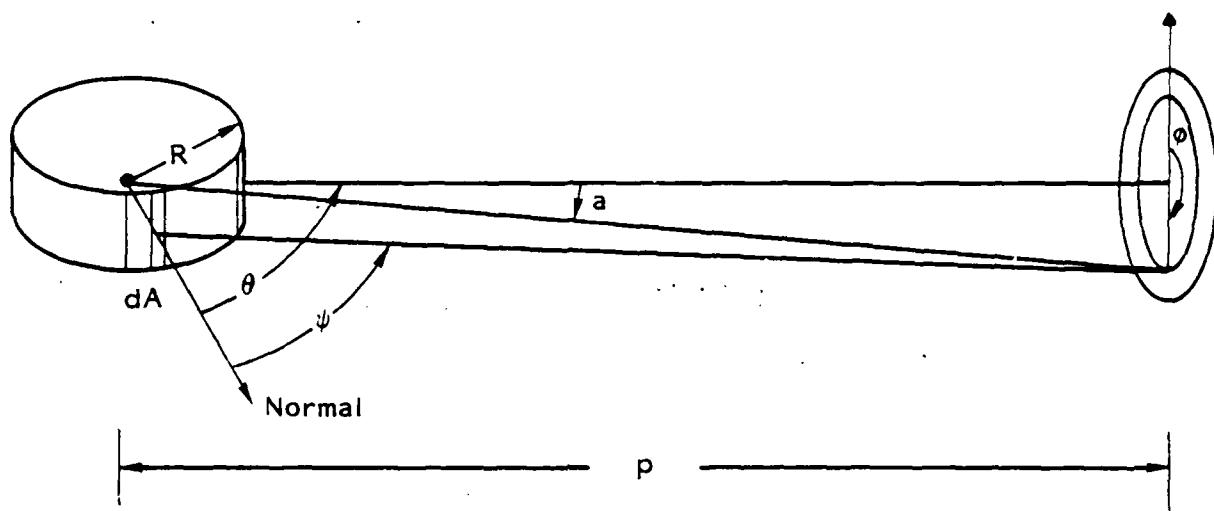
Figure 17. Geometry for illumination of camera by cylinder.

31

constant ($^-10^{12}$ for T in eV), and L = S/π since the black body emitter obeys Lambert's law. Thus, W = $2\pi^2$rL, and, inserting the transmission factor t,

$$W = \pi^2 R^2 I/(\ell t) = 8\pi ri/t \ (f/D)^2. \tag{12}$$

This is the required relation for channel emission W from the data i and r. The latter may be found from the image size s, knowing the camera system magnification, sr = mr and m = f/R.

4.5 OPTICALLY THIN CYLINDRICAL CHANNEL

As above, we must find a new relation between W and L(0), as well as a relation between i and L(0). In a plane perpendicular to the channel axis, we have an L(θ) proportional to cos θ; in a plane containing the channel axis, we have L(θ) proportional to sec θ. Note that the film image, if it were to possess sufficient resolution, contains information about the optical depth of the channel; if the channel limb-darkening corresponds to a cos(θ) law, we may take the channel as thin. If the brightness seems constant across the channel cross-section, we may treat it as optically thick. Unfortunately, in typical cases films have one to three grains across the channel. Consequently, theory must be used to estimate the optical depths in the spectral regime of interest (film response). That will not be treated here.

Assuming the channel is optically thin, we acquire (per unit length), to a good approximation, an addition factor of cos(θ) in the integral relating F to L(0). The integral over θ is now $\pi/4$, not 1 as in the optically thick case. This is a decrease of only 21%. We have in general I = eL(0)A/R^2 where e = 1 in the thick limit and $\pi/4$ in the thin limit. For the thin case, the loss rate per unit length W (W/m) = $\varepsilon \pi r^2$ where ε is the volume emissivity in watts per meter^3. We know that L(0) = 2r $\varepsilon/4\pi$, because the optical path length is 2r for $\theta = \phi = 0$, and each volume element along that path radiates isotropically over 4π steradians. Consequently, a volume element dV contributes εdV/4π watts/steradian to the radiant intensity in any direction. Note that as the radiant intensity

32

contribution of any element is independent of the distance from that element, we may simply integrate along the line of sight to obtain the radiant sterance in any direction. Thus, in the optically thin case, $W = L(0) \; r2\pi^2$, as in the thick case. Then

$$W = \pi^2 I R^2 / (e\ell) \; . \tag{13}$$

Finally $i = \pi e/4 \; L(0) \; (D/f)^2$ yielding the answer $W(Watts/m) = i(Watts/m^2) \times (f/D)^2 \; 8\pi R/(et)$. Given I or i, there is at most a 21% error in estimating W, given uncertainties in the channel optical depth.

The power incident at a detector of area A is $P = AI$. Thus, in general,

$$P = \frac{ew\ell}{\pi^2 R^2}$$

where
$$e = 1 \; \text{thick channel}$$
$$4/\pi \; \text{thin channel}$$

or

$$P = \frac{W\ell}{4\pi R^2} q \qquad q = 1 \; \text{thin channel}$$
$$4/\pi \; \text{thick channel}.$$

This result ($q = 1$) is used above in the analysis of Lite Mike data.

In many applications the result of a microdensitometer scan across the channel will be the observable: $B \; (W/m) = \int i \; dx$. For an optically thick channel there is no limb darkening and $B = iw$ where w is the image width of the channel. For a thin channel, while the image brightness will vary as $\cos(\theta)$, if we define w similarly we will have the same relationship between B and i. This is because luminance is conserved (except, of course, for the losses accounted for by the transmission factor t) and the relationship between image flux density and entrance pupil flux density and entrance pupil flux is unchanged (Ref. 9). One may also argue from a conservation of energy viewpoint. Thus, we find

$$W = \frac{f^2}{D} \frac{8\pi Bh}{t} \frac{R}{w}$$

where h = 1 if the channel is thick and $4/\pi$ if thin. But $2R/w = p/f = 1/m$ (see Section 4.4), so that

$$W = \frac{4\pi h}{t} \frac{fp}{D^2} B. \tag{14}$$

Note W may be inferred from B without knowledge of the channel radius, with channel optical depth introducing *only a small uncertainty if unknown.*

The optical depth of the channel must, however, be known to find h, and the spectral characteristics of the radiation must be known to relate the radiant quantities (i.e., those specified in Watts) to the film response.

4.6 SIMPLER DERIVATION BASED UPON SYMMETRY

We assume that a section of a lightning channel has been photographed and that the section of channel posesses axial symmetry with the axis perpendicular to the line from the section of channel to the camera lens.

We snall obtain the output power passing through the surface of a section of length ℓ of the channel by integrating the corresponding irradiance over the surface of a sphere of radius R, that is centered at the section of channel. The camera aperture diameter, D, is small compared to R. Therefore I, the irradiance (total flux per unit area), is uniform across the camera lens, and corresponds to the irradiance at 90° to the channel axis. Consider a detector measuring the irradiance at a point on the surface of the sphere. Let θ and ϕ be the coordinates of the point on the sphere. The angle the line from the center of the section of channel to the detector makes with the channel axis is θ, and the angle about the channel axis is ϕ. The irradiance, I, is independent of ϕ but will, in general, depend on θ. I is the radiant incidence or irradiance; it is the flux per unit area at a point on the sphere that come from all locations within the lightning channel. We can limit our discussion to I_ℓ, the

irradiance passing through the surface of a short length ($\ell \ll R$) of the channel, by considering only the photographic image of that portion of the channel.

For visible wavelengths, the channel is optically thin. The irradiance from the length of channel is proportional to the solid angle subtended by the length of channel as seen from the viewing location,

$$I_\ell \propto \sin \theta.$$

For an optically thin channel, the irradiance is proportional to the average path length, within the section of channel of rays arriving at the viewing location,

$$I_\ell \propto \frac{1}{\sin \theta}.$$

Therefore, for an optically thin channel, $I_\ell(\theta)$ is independent of θ,

$$I_\ell(\theta) = I_\ell(90°)$$

and W, the power output of the channel in watts per meter may be obtained by integrating I_ℓ over the surface of a sphere of radius R.

$$W = 2 \frac{R^2}{\ell} \int_0^{\pi/2} d\theta \int_0^{2\pi} d\phi \, I_\ell(90°) \sin \theta \tag{15}$$

$$W = \frac{4\pi R^2}{\ell} I_\ell(90°) \int_0^{\pi/2} d\theta \sin \theta = \frac{4\pi R^2}{\ell} I_\ell(90°). \tag{16}$$

Equations 16 and 13 agree.

The irradiance at the camera lens is obtained by integrating I_f, the irradiance at the film over the image of the channel section.

$$I_\ell(90°) = \frac{1}{A} \int_0^{M\ell} dy \int_{-a}^{a} dx \, I_f \tag{17}$$

35

where M is the image magnification, y is the direction along the channel, x is across the channel, and A is the area of the camera aperture. The assumption that I_f is independent of y leads to the simplification

$$I_\ell = \frac{M\ell}{A} \int_{-a}^{a} I_f \, dx .$$ (18)

The integral immediately above may be evaluated even if the channel is not well-resolved due to the graininess of the photograph. The equation for the power output per unit channel length is

$$W = \frac{4\pi R^2 M}{A} \int_{-a}^{a} I_f \, dx .$$ (19).

The integration limit, a, must be taken large enough to include the width of the channel on the photograph.

Introducing N = the camera f-number, F = the camera focal length, and D = the camera aperture diameter, the camera aperture area is

$$A = \frac{1}{4} \pi D^2 = \frac{1}{4} \pi N^2 F^2$$

and the magnification is

$$M = F/R .$$

The channel radiated power per unit length is

$$W = \frac{16R}{N^2 F} \int_{-a}^{a} I_f \, dx .$$ (20)

Equation 20 is our main result.

It may be of interest to obtain W for an optically thick channel. The the irradiance at an observation point originating at the surface of the segment of channel is

$$I_\ell(\vartheta) = I_\ell(90°) \sin \vartheta$$ (21)

because the intensity of a ray is independent of the distance it has passed through the hot gas. The power output of the channel is

$$W = 2 \frac{R^2}{\ell} \int_0^{\pi/2} d\theta \int_0^{2\pi} d\phi \; I_\ell(90°)\sin^2\theta$$

$$W = \frac{4\pi R^2}{\ell} I_\ell(90°) \; d\theta \int_0^{\pi/2} \sin^2\theta$$

$$W = \frac{\pi^2 R^2}{\ell} I_\ell(90°) \; . \tag{22}$$

Equations 26 and 12 agree. Therefore, for an optically thick channel, we use Equations 18 and 22 to obtain

$$W = \frac{M\pi^2 R^2}{A} \int_{-a}^{a} I_f \; dx \tag{23}$$

or

$$W = \frac{4\pi R}{N^2 F} \int_{-a}^{a} I_f \; dx \tag{24}$$

where W is in watts per meter. Equation 24 gives the power output for an optically thick channel, and is a factor of $(\pi/4)$ times the power radiated by an optically thin channel (Eq. 20). In applying Equations 20 or 24, it is not necessary to determine the width of the channel, nor is it necessary to resolve the brightness at a specific point on the channel.

4.7 CONCLUSION

The principal conclusion is that optical observations of lightning can yield accurate energy loss rates without knowledge of channel radius or optical depth. The formulae above are ready for application. Only the optical depth in the spectral region of interest is needed, as well as estimates of the channel radius (uncertain due to film resolution by a factor of roughly two to three). Note that Equation 20 or 24 may be applied to a case in which the channel radius is not resolved, without the

37

necessity of estimating the channel radius. The parameter E may be inter-
polatedas a function of optical depth for the cylindrical case as in the
slab case; optical depths of a few are indistinguishable from infinite
optical depth, depths smaller than one are qualitatively similar to the
thin limit. Even a poor estimate of the channel optical depth will yield
an accurate loss rate. The atmospheric transmission is another
uncertainty.

5. ANALYSIS AND INTERPRETATION OF B-DOT SIGNALS

5.1 RESULTS OF COMPUTER MODELING OF FIELDS FROM THE STROKE CURRENT

The Lite Mike experiments provided data from B-Dot and D-Dot sensors located at Kiva 1, in addition to the Lite Mike and current sensor data. It was felt that it would be of interest to analyze these data records. While a great deal of data from these sensors have been reported in Lightning Phenomenology Note 3 and Lightning Phenomenology Note 11, a detailed analysis of these data does not seem to have been performed for any cases yet. We hope that the results presented here stimulate the application of sophisticated models to the treasury of data from the Kivas. One novel discovery, that of a higher initial return stroke velocity than previously observed, has been made. It is necessary to confirm this result with additional observed cases. The confirming data may already exist, and merely await detailed analysis.

The strike of record 85220 will be analyzed. It appears to be rather typical of strikes. There are two strikes for 85222; these posses anomalously low current amplitudes of about 2000 A maximum. Furthermore, the B-Dot and D-Dot records have not been made available for analysis.

The measured current of strike 85220 is shown in Fig. 6. The polarity is positive vertical current (i.e., the lowering of negative charge or the rise of positive charge), whicn is the most common form for rocket-triggered lightning. This current was modeled for computational purposes as a double exponential waveform, shown in Fig. 18. The fall time is not important as the results are most sensitive to the rise time.

Videotape observations show that the stroke was approximately vertical within the vicinity of the stinger, witn an inclination of approximately 15 degrees to the vertical, the channel moving toward the southeast with increasing height. We will consider a vertical channel, and treat the inclination of the channel through an approximation. The vertical

39
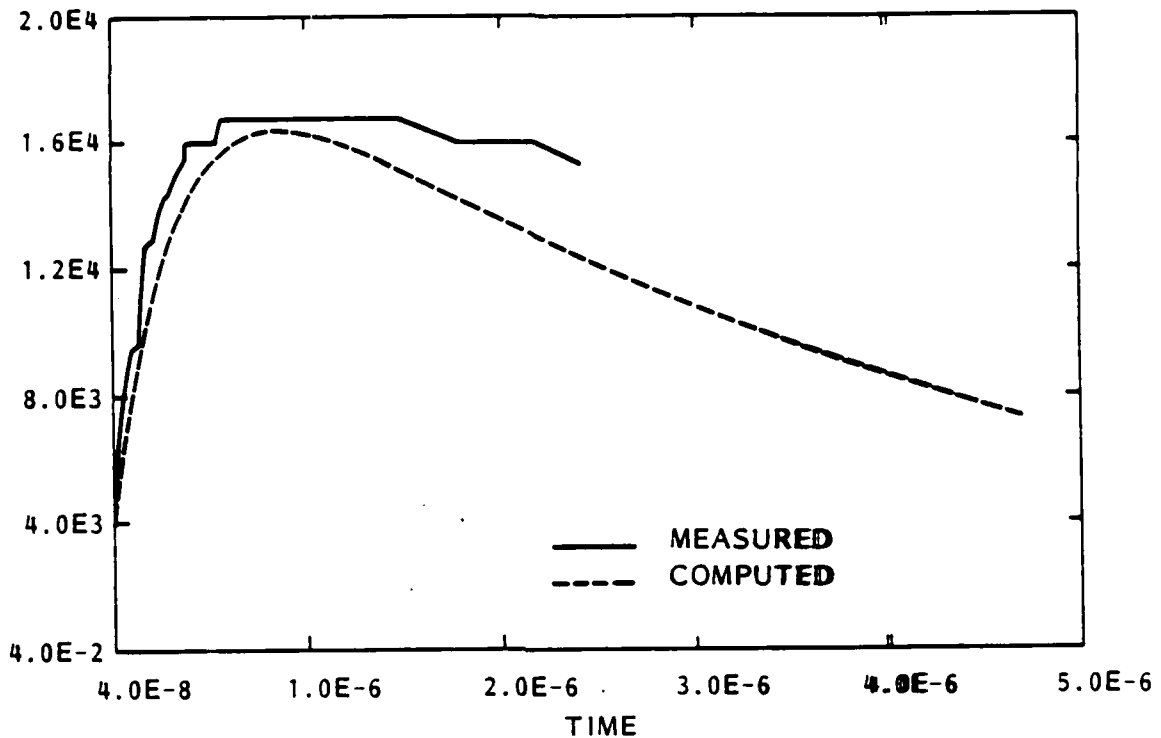
Figure 18. Measured and computed current in channel
versus time.

component of the current will be used to compute the vertical electric dis-
placement and the azimuthal magnetic induction at the location of the sen-
sors, and the distance will not be measured from the vertical line but from
the displaced channel location, taken to be in the EW plane.

The basic method is that of Uman, McLain, and Krider (Ref. 10), who
consider an ideal (lossless) transmission line with the current waveform
propagating upward without modification. The ground is assumed to be per-
fectly conducting, producing ideal image currents in the ground plane.
Because of the conducting wire grid in the area of the stinger, this should
be an excellent approximation. The ground is not perfectly flat or uni-
form, with the sensors at Kiva 1 approximately 4 m below Kiva 2. The sen-
sors will be assumed to be 40 m from the channel base. The stinger height
is 20 m. To take full account of the physics of stroke initiation, one
would have to consider not one wave travelling upward from the ground (and

40

its image), but one wave starting upward from the initiation point, and another starting downward from this point. These waves would have images. In addition, the downward wave would be reflected from the ground, giving rise to an upward wave. To a good approximation, these added complications may be ignored after the transit of the wave back to the initiation point, i.e., after a time $2H/c$, where H is somewhat greater than 20 m and c is the speed of light. This time is roughly 130 ns. We will make this approximation, which is justified a posteriori by the agreement of the observations and computational results. The wave is assumed to propagate at a velocity V.

The azimuthal magnetic induction B is the sum of two terms, an induction term and a radiation term, the former having an inverse square dependence upon distance from the radiating element, and the latter an inverse dependence upon distance. This results in the radiation term dominating at very large distances. At the very close distances of interest here, the terms are of comparable magnitude. At very early times, the terms are both positive with the radiation term dominating due to the rapidity of the field changes. After 400 ns in the case computed and displayed in Figures 19 through 22, the induction term is larger than the radiation term. At late times (after 1.7 μs for the V = 0.9 c wave velocity case considered here) the radiation term becomes negative, but it typically remains an order of magnitude smaller than the induction term. The full expression for B is .

$$B_\phi(D,t) = \frac{\mu_0}{2\pi} \int_0^H \frac{\sin\theta}{R^2} \, i(z, t - R/V)dz$$

$$+ \frac{\mu_0}{2\pi} \int_0^H \frac{\sin\theta}{cR} \, \frac{\partial i(z, t - R/V)}{\partial t} \, dz \tag{25}$$

where θ is the angle between the channel and the radius between the radiating element and the observation point on the ground plane. Thus, each term is positive and decreases rapidly as we go up the channel, both because of the factors of R and the factor of $\sin(\theta)$.
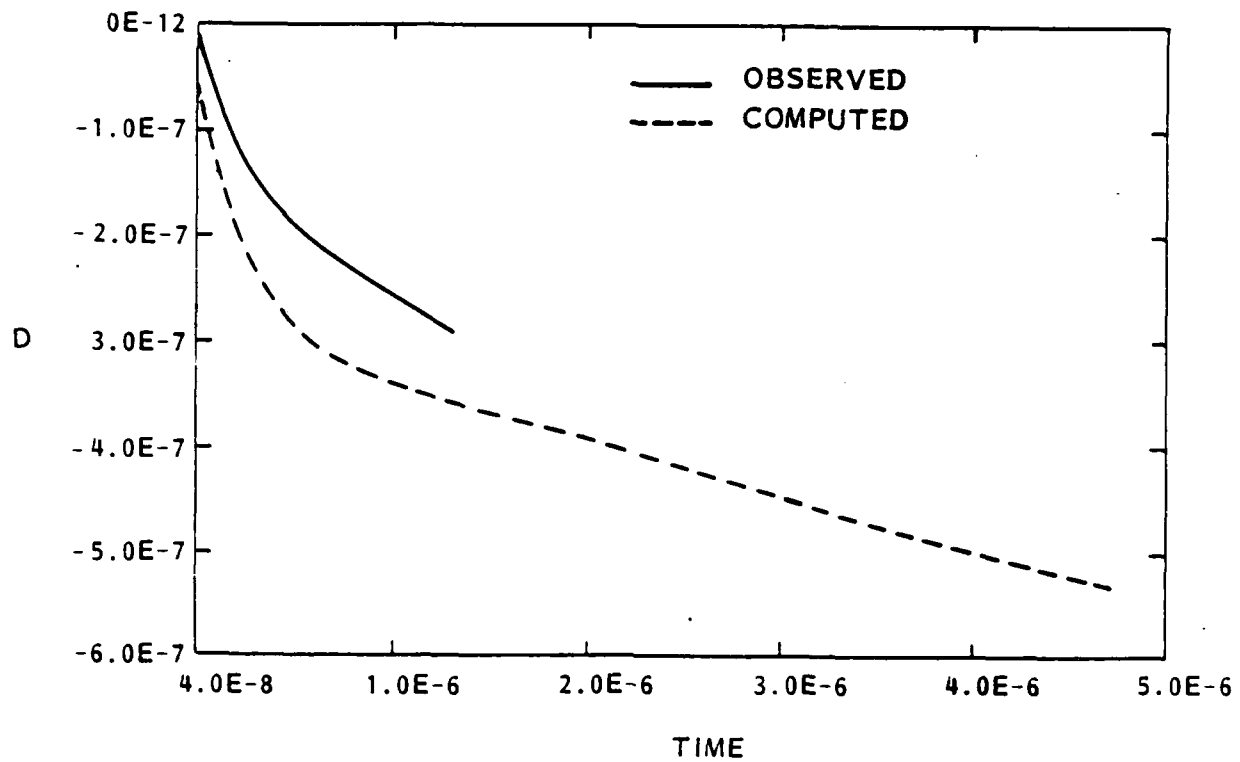
Figure 19. Observed and computed electric displacement
D versus time for wave velocity 0.9 c.
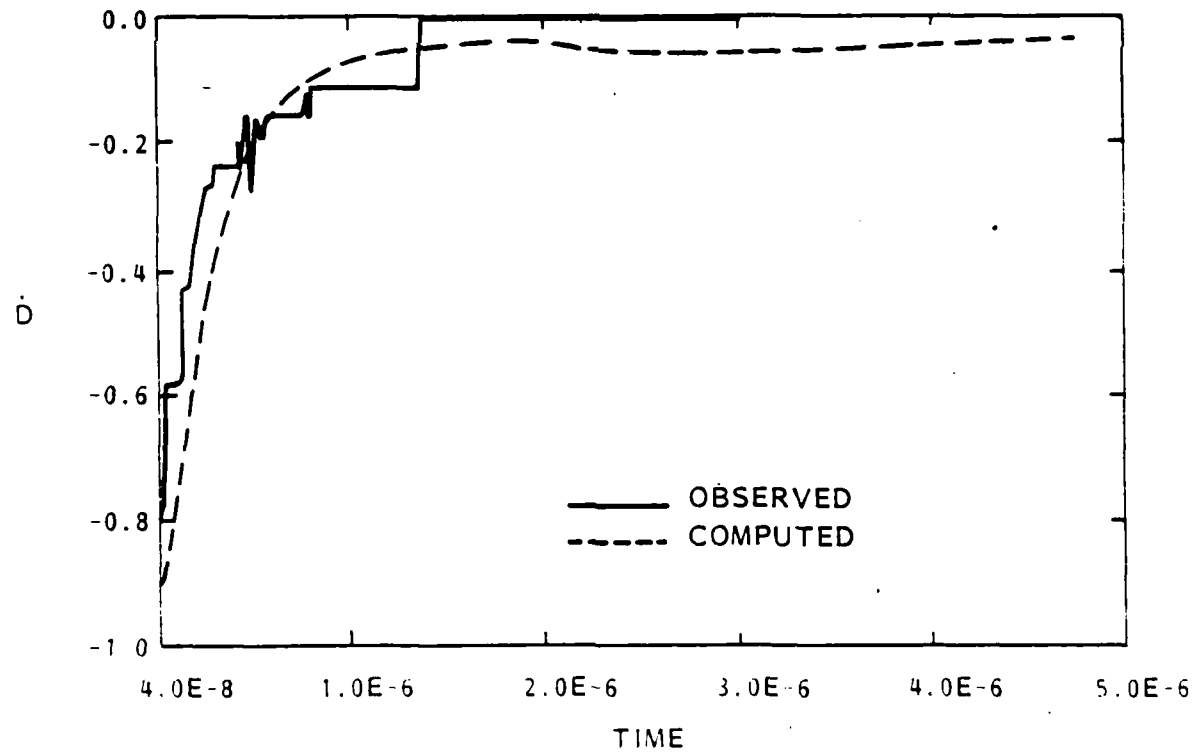
Figure 20. Observed and computed derivative of electric
displacement, Ḋ.

42
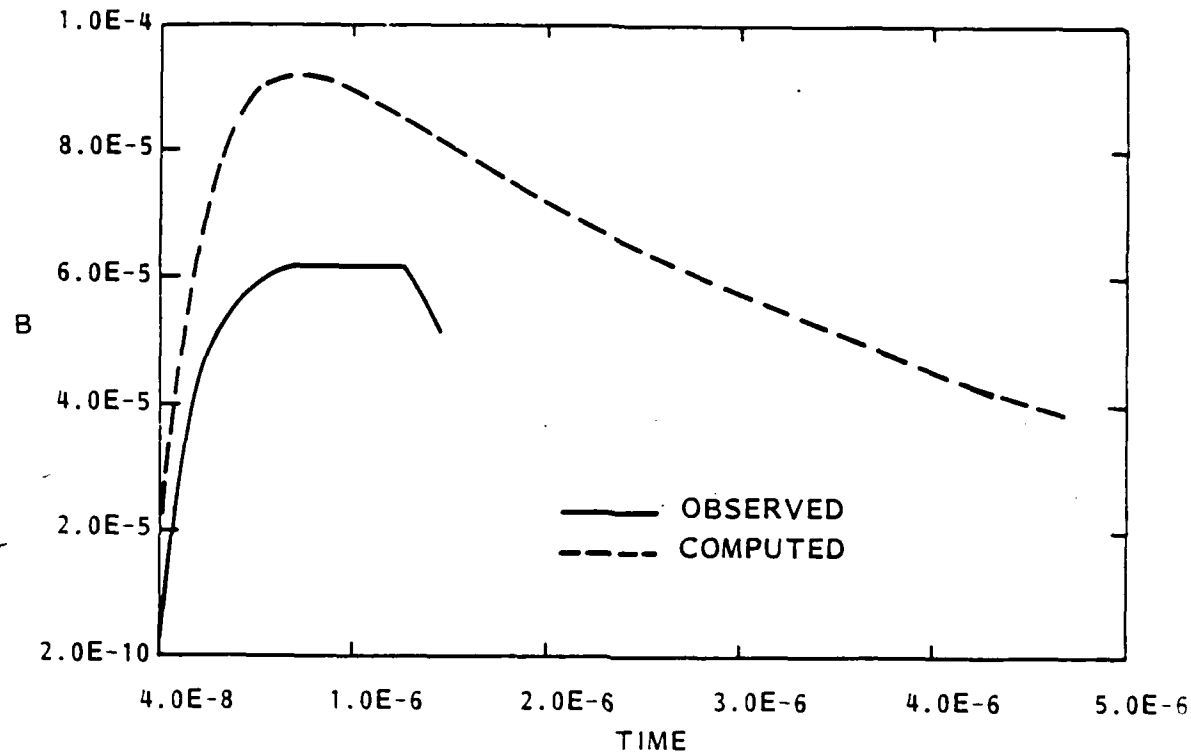
Figure 21. Observed and computed magnetic induction B
versus time for wave velocity 0.9 c.

The electric field is more complicated, having a static term, an
induction term and a radiation term:

$$E_z (D, t) = \frac{1}{2\pi\varepsilon} \left[\int_0^H \frac{(2 - 3 \sin\theta)}{R^3} \right.$$

$$x \int_0^t i(z, \tau - R/V) \, drdz$$

$$+ \int_0^H \frac{(2 - 3 \sin\theta)}{cR^3} i(z, t - R/v) \, dz$$

$$\left. - \int_0^H \frac{\sin\theta^2}{c^2R} \frac{\partial i(z, t - R/V)}{\partial t} \, dz \right] . \qquad (26)$$

43
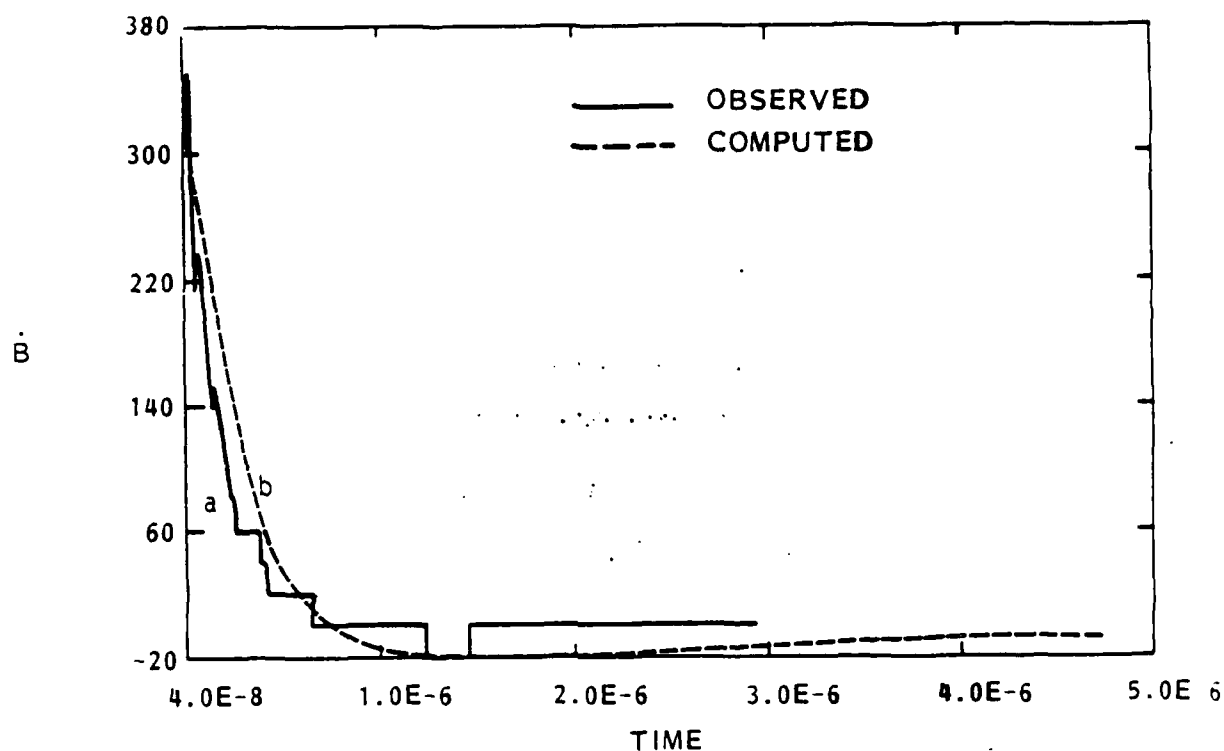
Figure 22. Observed and computed derivative of magnetic
induction, Ḃ.

The static term is due to the effective dipole moment formed by the moving current pulse and it image, which results in a $1/R^3$ dependence. This term does not vanish at large times due to the finite charge transported by the stroke. All the terms contributing to the electric field

44

and electric displacement have much stronger dependences upon channel height, due either to a factor of $\sin^2\theta$ instead of sin in the radiation term or factors of $2-3\sin^2\theta$ in the other terms, and the R^3 dependence of static field term. Note that the static and induction field terms are of indefinite sign. Lower levels of the channel have values of $\sin\theta = D/R$ close to one, giving a negative contribution. Higher portions of the channel have small values of the sine term, giving a positive contribution. The factor $(2-3\sin^2\theta)$ does not vanish with height as do the factors of sin in the terms for B, so the induction term might be more significant than the corresponding term in the equation for B. The crossover occurs at a height of 1.414 D, where D is the distance of the observer from the channel base. In our case this is a mere 60 m or so. It is seen from the downward nature of D and E for upward current that the portions of the channel below this height dominate in their contributions in the measured signal. However, the static term is found to dominate the other terms except at very early times, at which all play a role. Initially, all terms are negative, with the radiation term dominant due to the large time derivatives. Soon the static term dominates, on the same timescale as the induction term in the magnetic induction dominates the radiation term. Both the induction and radiation terms change sign, the former at 1 μs and the latter at 1.4 μs in the case of Figs. 19 through 22. The static term is about one order of magnitude larger than the induction field which in turn is one order of magnitude larger than the radiation term. Obviously, these relationships will change if the observer is located farther from the the channel or if the current pulse differs.

For computational purposes, the radiation terms were integrated by replacing the time derivative of the current with the derivative of current with respect to height. Thus, the second integral in the expression for B becomes

$$-\frac{\mu_0 v}{2\pi c} \cdot \frac{\sin\theta}{R} \, di \qquad (27)$$

which may be integrated by parts to yield

$$\frac{\mu_0 V}{2\pi c} \quad \frac{D}{(D^2 + z^2)} \quad i + v \int i \frac{d}{dz} \frac{(\sin\theta)}{R} dz. \tag{28}$$

The radiation term in the equation for the electric field is similar except that $\sin^2\theta$ replaces $\sin\theta$. With the substitution $\sin\theta = D/R$ and $R = \sqrt{(D^2 + z^2)}$ we may calculate the derivative in the integral, which is $-2z/(D^2 + z^2)$ for the expression above.

The static field term is calculated by defining a variable $q(z)$ as the time integral of the current at any height. As the observer is stationary, this suffices because the retardation to any point on the channel does not change.

In the transmission-line model the principal free parameter (once the waveform of the current pulse, which is completely free, is specified), is the wave velocity. Good agreement was found for the model used with a wave velocity of $V = 0.9$ c, where c is the speed of light. We present the results for this assumed wave velocity as follows: Fig. 19 compares observed and computed electric displacement D; Fig. 20 compares D-Dot; Fig. 21 compares magnetic induction B, and Fig. 22 B-Dot. Note that the sensor for D-Dot causes a sign change between the computed and observed results for these quantities.

Figures 23 through 26 give results for computed fields with an assumed wave velocity of c/3. It will be seen that the peaks in the derivative signals are delayed and reduced in magnitude, resulting in poorer agreement with observations.

5.2 INTERPRETATION OF RESULTS

The wave velocity which best matches observations is higher than typically reported for return strokes. Uman (Ref. 11) gives c/3 as a typical values and c/2 as a typical upper limit to reported velocities.
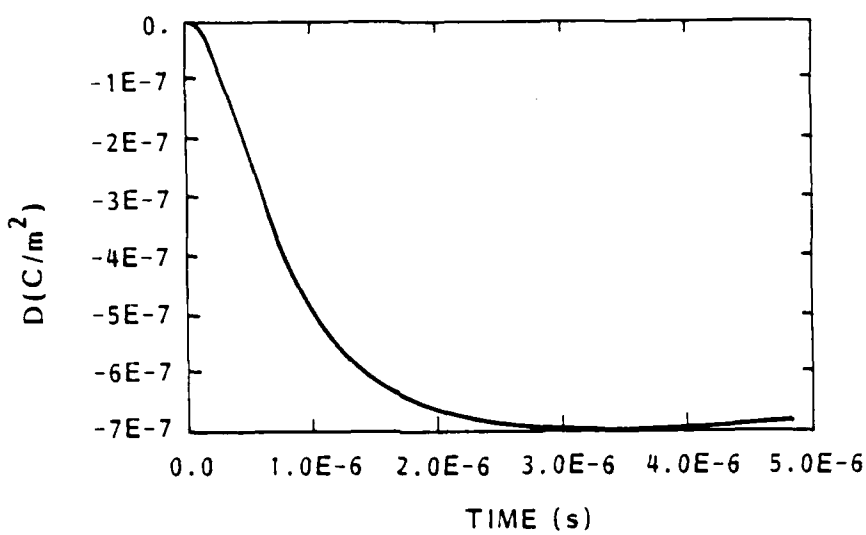
Figure 23. Computed results for wave velocity c/3:
Electric displacement D.
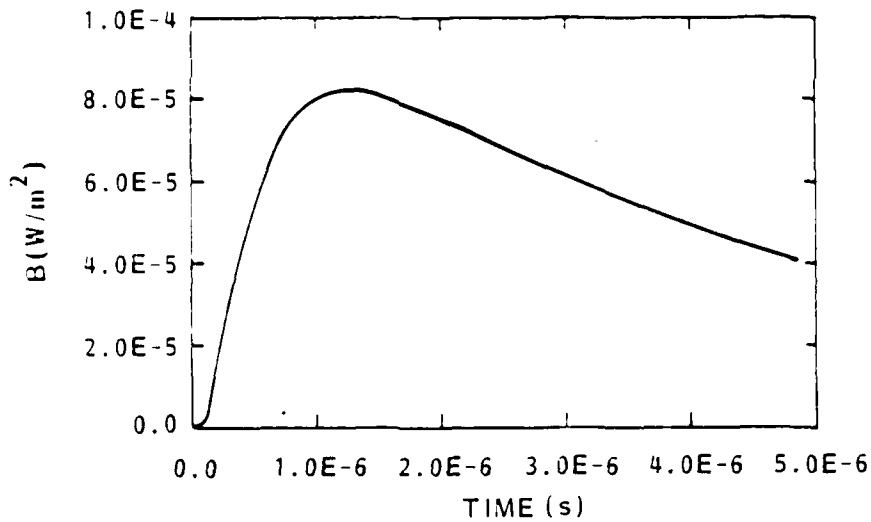

Figure 24. Computed results for wave velocity c/3:
Magnetic induction B.

47
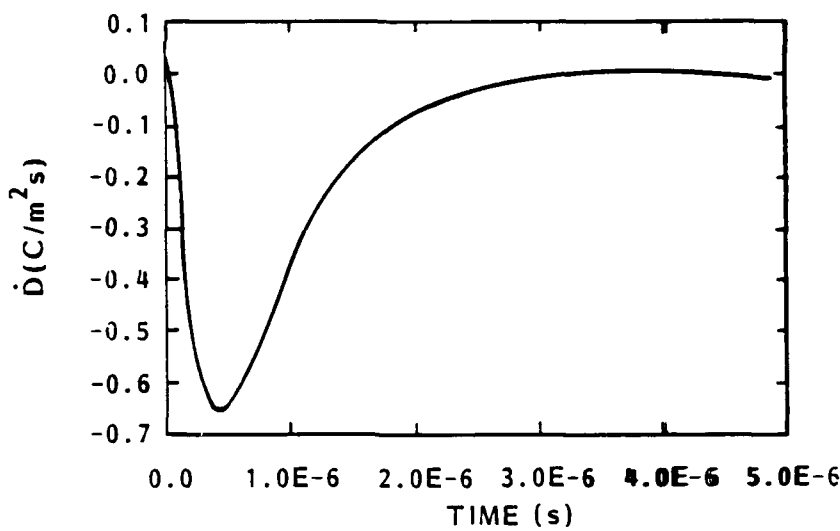
Figure 25.   Computed results for wave velocity c/3:
Derivative of electric displacement, $\dot{D}$.
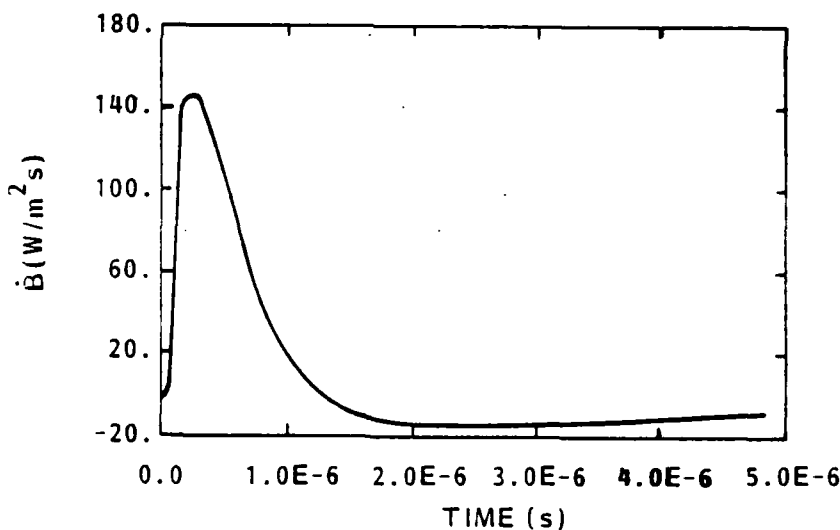
Figure 26.   Computed results for wave velocity c/3:
Derivative of magnetic induction, $\dot{B}$.

48

The explanation most likely is that near the ground the velocities are higher than average. The wave is traveling in the most recently formed portion of the channel, which is probably still highly conductive and which has not dispersed to any degree. As the wave progresses, it encounters channel segments which have cooled and undergone attachment, recombination and some hydrodynamic dispersal due to turbulence, etc. The corona envelope which would store the charge around the channel is probably of greater diameter as well as more resistive due to attachment. This would account for the reduced wave speed (Refs. 12, 13).

The high wave velocity is also of great interest as it results in a correspondingly larger value of radiated fields for a given current than for low wave velocity. This is of importance in comparing the I of return strokes inferred by different methods (e.g., remote and tower measurements) (Ref. 14).

In the present work, it has been adequate to assume constant wave speed and wave shape to obtain reasonable agreement with observation. Residual errors might be explained due to the imperfect ground plane (neither flat nor perfectly conducting) and the non-ideal channel geometry (not perfectly vertical). Because, as noted above, the very lowest portions of the channel are dominating the signal, it is quite possible that the wave has moved beyond this region of importance before it has changed significantly in profile or velocity. As this region of significance is roughly the lowest 60 m of the channel, 20 m of which is contributed by the stinger, this should not be surprising.

The details of wave initiation, which would influence the first 10 ns or so of the signal, do not seem to be important in contributing to the observed fields.

49

5.3 CONCLUSIONS AND RECOMMENDATIONS

Based on these results, we would conclude the following:

(1) Near field values (B and D) can be adequately explained with simple models.

(2) Wave velocities near the ground appear to approach the speed of light. As this is significantly higher than reported wave velocities in the literature for return strokes; this suggests that the wave slows as it rises. It is quite plausible that the wave changes profile as well as it rises. This can be computed self-consistently (Ref. 13). Such a computation is not necessary for explaining the fields at a sensor 40 m from the stinger, as only heights of order 60 m or below contribute significantly to the fields here.

We would recommend for future investigations the following:

(1) Analyses similar to that performed here for B-Dot an D-Dot data as contained in Lightning Phenomenology Note 11 for selected strikes. This would give insignt into stroke initiation behavior. Such a series of analyses would confirm or refute the high initial wave velocities discovered in this work, and would thereby contribute new facts to the understanding of the lightning return stroke.

(2) More sophisticated analysis using the transmission-line model of Ref. 13. This would verify the hypothesis of the slowing of the wave with increasing channel height. Most importantly, it would enable us to build a model in which the wave shape is not arbitrary but determined by the physics of the lightning channel.

(3) Locating other sensors at greater distances from Kiva 2 to obtain information on the wave character at greater heights. This would be useful only if better information on channel geometry were available as well. This information might in part be obtained by locating sensors at different azimuths from the stinger, but probably would require more videotape locations.

6. LIGHTNING PROTECTION AND TRIGGERING ANALYSIS

Lightning protection is usually accomplished by providing an alternate path for the discharge. The alternate path must include an electrode that will form a leader and connect with any lightning leader before a leader from the protected object can do so. The question of whether or not a leader from an electrode will be formed and sustained by a given gap voltage and geometry is also of interest in the analysis of lightning triggering. The structure of an empirical model for lightning assessment is described in Section 6.1. There are unknown parameters that must be provided for the model by performing experiments with long spark gaps; or, it may be possible to deduce the parameters after conducting a thorough search of the literature that is available on the breakdown of long spark gaps.

The charging rate of a grounded imperfect conductor suspended in a vertical gap is discussed in Section 6.2. This analysis is related to the question of whether or not the channel formed by the detonation of a suspended detonating fuse would retain its conductivity for long enough for charge to accumulate at the upper end so that an upward leader could be launched.

6.1 EMPIRICAL MODEL FOR LIGHTNING PROTECTION

A model for lightning protection assessment is concerned with positive streamers that are launched by objects near the ground. In experiments conducted with long sparks, a given voltage waveform will have a probability of causing a breakdown of the gap. There is also a statistical distribution of the time to leader inception and the time to breakdown. For protecting high-voltage transmission lines from breakdown, it is only important to treat the probability of breakdown of a given gap. Semi-empirical models are well developed for this case. For the case of lightning protection, however, the voltage at the lightning rod and the protected conductor continues to increase as the cloud to earth leader approaches until an upward leader from one of them reaches it and causes a

conducting path to ground. Therefore, the probability distribution of the relative times at which leader inception occurs at the two conductors is a crucial consideration for the lightning-protection case, and the existing models can not be used.

Reference 15 includes a brief discussion of the time to breakdown of air gaps. We assume a configuration consisting of a lightning rod of height h_r, a protected object of height h_p, and a negative leader approaching with speed v from above at height h_ℓ at time $t = 0$. Usually, we expect that $h_\ell \gg h_r > h_p$. A positive leader will be launched by the object or by the lightning rod, or by both. At least one of the positive leaders will join the negative leader, determining where the lightning will strike. To illustrate the general method proposed, it is assumed that the voltage between the positive leader and the lightning rod is, to first order,

$$U_r(t) = \frac{U_1}{d_1 - vt} \tag{29}$$

where $d_1 = h_\ell - h_r$. Similarly, the voltage between the positive leader and the object is

$$U_p(t) = \frac{U_2}{d_2 - vt} \tag{30}$$

where $d^2 = h_\ell - h_p$. The time to breakdown of air gaps can be fitted to a Weibull distribution for the probability density (Ref. 15).

$$p(y) = (\alpha/\tau) \, y^{\alpha-1} \, \exp(-y^\alpha) \tag{31}$$

where $y = (t-\varepsilon)/\tau$, typically, α is given the value $\alpha = 1.5$, and ε represents a minimum time for breakdown. ε and τ are functions of the breakdown overvoltage factor

$$f = \frac{U}{U_s} \tag{32}$$

where U_s is the voltage resulting in a probability distribution with "width" τ_s. Looking at plots in Ref. 15, we surmise that

$$\tau \cong \tau_s \, e^{-\beta(f-1)} \tag{33}$$

and

$$\varepsilon \cong \varepsilon_0 + \varepsilon_1 \, e^{-\rho(f-1)} \tag{34}$$

provide a reasonable fit to the data.

The probability of breakdown between the positive leader and the lightning rod, during an elapsed time t is

$$P_1(t) = \int_0^t n[t' - \varepsilon_1(t')] \, [\alpha/\tau_1(t')] \, y_1^{\alpha-1} \, \exp(-y_1^{\alpha}) dt' \tag{35}$$

where n is the unit step function

$$n(z) = \begin{array}{ll} 1 & \text{for } z > 0 \\ 0 & \text{for } z < 0 \end{array} \tag{36}$$

and τ_1, ε_1, and y_1 are obtained by substituting Equation 36 into Equations 31, 32, 33 and 34. A similar equation may be obtained for $P_2(t)$, the probability that breakdown occurs between the positive leader and the protected object before time t.

This is only the outline of a possible semi-empirical model for lightning protection. Verification of the forms of the equations and the evaluation of ε_0, ε_1, τ_s, β, and ρ for various electrode geometries would require a detailed survey of the available data on breakdown conditions for long sparks. More than one parameter, e.g., pulse rise time and peak voltage, are frequently varied from measurement to measurement, so the dependence on a single variable is frequently difficult to extract. The type of measurement that would be the most useful for lighting protection problems is not directly applicable to the breakdown of electrical power transmission networks, and is therefore rarely made. This is the

54

measurement of the time to breakdown as the voltage is increased at an approximately constant rate. The time to breakdown that occurs during the leading edge of a switching impulse may be a suitable substitution for this type of measurement, however.

6.2 RATE OF VOLTAGE CHANGE AT THE END OF A VERTICAL HIGH-RESISTANCE CONDUCTING CHANNEL CREATED BY THE IGNITION OF A SUSPENDED DETONATING FUSE

It has been suggested that lightning could be triggered by suspending a long section of grounded detonating fuse from a balloon and igniting it (Ref. 16). The channel created by the ignition has a resistance of about 2 $k\Omega/m$ for a duration of 7 ms. The question addressed here is whether or not this is sufficient time for the upper end of the fuse to reach a potential that is nearly the same as the ground potential.

The equation for the potential of a transmission line is

$$\frac{\partial^2 V}{\partial Z^2} = LC \frac{\partial^2 V}{\partial t^2} + RC \frac{\partial V}{\partial t} \tag{37}$$

where L, R, and C are assumed to be slowly varying in time and space. If $R \gg \omega L$ for frequencies ω of interest, the first term on the right-hand side of Equation 37 may be neglected.

$$\frac{\partial^2 V}{\partial Z^2} = RC \frac{\partial V}{\partial t} \tag{38}$$

Equation 38, the one-dimensional diffusion equation, may be solved using the technique of separation of variables. The length of the conducting channel ℓ is small compared to the distance separating the earth and the charge pocket in the cloud; therefore, C is approximately constant over the length of the channel (Ref. 17).

The initial condition is $V_0(z) = Uz/\ell$ and the boundary conditions are $V(0, t) = 0$ and $V(\ell, t) = 0$. The steady-state solution is $V(z, t = \infty) = 0$. Separation of variables takes the form $V = \rho(t) V_0(z)$.

Equations for V_0 and ρ are

$$\frac{d^2 V_0}{dz^2} = V_0 n^2 \tag{39}$$

and

$$\frac{d\rho}{dt} = \frac{n^2 \rho}{RC} \tag{40}$$

where n is the separation constant. By expanding V_0 as a Fourier series and solving Equation 40, a series solution is obtained,

$$\cdot \; V = 2a \sum_{n=1}^{\infty} \frac{(-1)^n}{n} \sin (n\pi z/\ell) \exp -(n^2\pi^2 t/\ell^2 RC) \quad \cdot \tag{41}$$

where $a = u/\pi$. The time constant for the exponential decay of the end of the channel to zero potential is $\ell^2 RC/\pi^2 = (500 \text{ m})^2 (2\times10^3 \Omega/\text{m})\times$ $(5\times10^{-12}\text{f/m})/\pi^2 = 0.25$ ms. Therefore, the lowest Fourier component will decay to e^{-1} of its initial amplitude in 0.25 ms. Higher Fourier components will decay much faster. Therefore, there was plenty of time for *the upper end of the channel to reach essentially zero potential,* and the charging time required does not provide an explanation of the inability to trigger lightning in this manner. The current in the channel is

$$I = -\frac{1}{R} \frac{\partial V}{\partial Z} = 2D \sum_{n=1}^{\infty} (-1)^n \cos(n\pi z/\ell) \exp-(n^2\pi^2 t/\ell^2 RC) \tag{42}$$

where $D = a\pi/\ell R$. Equation 42 can be summed analytically,

$$I = D[\theta_4(u,q)-1] \tag{43}$$

where θ_4 is the theta function, $u = \pi z/2\ell$, and $q = \exp-(\pi^2 t/\ell^2 RC)$.

The time interval for which the detenoting fuse retained its conductivity was adequate for the potential of its upper end to be reduced nearly to ground potential; therefore, the failure of the detonating fuse to trigger ligntning can not be explained by an inadequate rate of charge transfer.

Although this analysis shows that the resistance of the channel formed by the detonating cord was low enough to produce electric fields adequate for the formation of an upward leader, additional analysis is necessary to determine if the resistance was too high to sustain the leader growth. This is a possible explanation of the failure to trigger lightning. It is also possible that the conducting channel was sufficient but the atmospheric conditions were not suitable for lightning formation. Lightning is not triggered by every wire-trailing rocket that is fired into a thunderstorm at the North Baldy site.

REFERENCES

1. Baum, C. E., et al., Lightning Current Measuring Sensor Array, Kiva Memo 4, C. E. Baum, Editor, Air Force Weapons Laboratory, Kirtland Air Force Base, N. Mex., October 1984.

2. Baum, C. E., et al., "Electromagnetic Sensors for General Lightning Application", in Lightning Technology, NASA Conference Publication 2128 FAA-RD-80-30, April 1980.

3. Baum, C. E. and J. P. O'Neill, Kiva 2, Kiva Memo 2, C. E. Baum, Editor, Air Force Weapons Laboratory, Kirtland Air Force Base, N. Mex., January 1984.

4. Baker, L., CHARTB Multigroup Transport Package, SAND-79-0386, Sandia National Laboratories, Albuquerque, N. Mex., March 1979.

5. Johnston, R. R., et al., Radiative Properties of High Temperature Air, LMSC D267205, Lockheed Palo Alto Research Laboratory, Palo Alto, CA, 1972.

6. Johnston, R. R., and D. E. Stevenson, Radiative Properties of High Temperature Air, II, SAI-056-77-PA, Science Applications, Inc., Palo Alto, CA, 1977.

7. Sears, F. W., et al., College Physics, 5th ed., Addison-Wesley Publ. Co., Reading, Mass., 1980.

8. Larmore, L., Introduction to Photographic Principles, Dover, New York, N.Y., 1958.

9. Williams, C. S., and O. A. Becklund, Optics: A Short Course for Engineers and Scientists, Wiley-Interscience, New York, N.Y., 1972.

10. Uman, M. A., et al., "The Electromagnetic Radiation from a Finite Antenna." American Journal of Physics, Vol. 43, pp. 33-38, January 1975.

11. Uman, M. A., Lightning, McGraw-Hill, New York, N.Y. 1969.

12. Baum, C. E., and L. Baker, Transmission-Line Model Return-Stroke, Lightning Phenomenology Note 13, Mission Research Corporation, Albuquerque, N. Mex., C. E. Baum, Editor, Air Force Weapons Laboratory, Kirtland Air Force Base, N. Mex., October 1984.

13. Baker, L., C. E. Baum, and R. L. Gardner, Review of Propagation Effects for Electromagnetic Pulse Transmission, Lightning Phenomenology Note 14, Mission Research Corporation, Albuquerque, N. Mex., C. E. Baum, Editor, Air Force Weapons Laboratory, Kirtland Air Force Base, N. Mex., January 1985.

REFERENCES (Concluded).

14. Gardner, R. L., et al., Comparison of Public Domain Hemp and Lightning on the Surface of an Aircraft, Lightning Phenomenology Note 12, Mission Research Corporation, Albuquerque, N. Mex., C. E. Baum, Editor, Air Force Weapons Laboratory, Kirtland Air Force Base, N. Mex., August 1984.

15. Jones, B. and R. T. Waters, "Air Insulation at Large Spacings" Proceedings IEE, Vol. 125 No. 11R, pp. 1152-1176, November 1978.

16. Moore, C. B., W. P. Winn, D. L. Hall, and J. W. Cobb, An Investigation into the Use of Detonating Fuses to Create Conducting Paths in the Atmosphere, Measurement Note 30, EMP Note Series, C. E. Baum, Editor, Air Force Weapons Laboratory, Kirtland Air Force Base, N. Mex., March 1984.

17. Little, P. F., "Transmission Line Representation of a Lightning Return Stroke." Journal of Applied Physics, Vol. 11, pp. 1983-1910, May 1978.

EMD

6 - 81

DTIC